THE JOURNAL OF PHYSICAL CHEMISTRY A
A JOURNAL OF THE AMERICAN CHEMICAL SOCIETY

pubs.acs.org/JPCA Article

Exploring the Photochemistry of Solid 1,1-Diamino-2,2-dinitroethylene (FOX-7) Spanning Simple Bond Ruptures, Nitro-to-Nitrite Isomerization, and Nonadiabatic Dynamics

Published as part of The Journal of Physical Chemistry virtual special issue "Marsha I. Lester Festschrift".

Andrew M. Turner,[#] Yuheng Luo,[#] Joshua H. Marks, Rui Sun,[*] Jasmin T. Lechner, Thomas M. Klapötke,[*] and Ralf I. Kaiser[*]

Cite This: https://doi.org/10.1021/acs.jpca.2c02696 Read Online

ACCESS | Metrics & More | Article Recommendations | Supporting Information

ABSTRACT: The UV photolysis of solid FOX-7 at 5 K with 355 and 532 nm photons was investigated to unravel initial isomerization and decomposition pathways. Isomer-selective single photon ionization coupled with reflectron time-of-flight mass spectrometry (ReTOF-MS) documented the nitric oxide (NO) loss channel at 355 nm along with a nitro-to-nitrite isomerization, which was observed by using infrared spectroscopy, representing the initial reaction pathway followed by O—NO bond rupture of the nitrite moiety. A residual gas analyzer detected molecular oxygen for the 355 and 532 nm photolysis at a ratio of 4.3 ± 0.3:1, which signifies FOX-7 as an energetic material that provides its own oxidant once the decomposition starts. Overall branching ratios for molecular oxygen versus nitric oxide were derived to be 700 ± 100:1 at 355 nm. It is notable that this is the first time that molecular oxygen was detected as a decomposition product of FOX-7. Computations show that atomic oxygen, which later combines to form molecular oxygen, is likely released from a nitro group involving conical intersections. The condensed phase potential energy profile computed at the CCSD(T) and CASPT2 level correlates well with the experiments and highlights the critical roles of conical intersections, nonadiabatic dynamics, and the encapsulated environment that dictate the mechanism of the reaction through intermolecular hydrogen bonds.

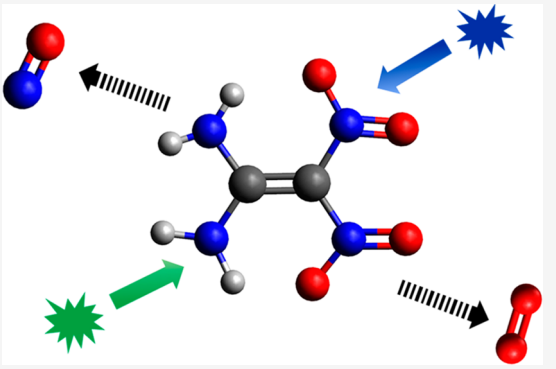

1. INTRODUCTION

An intimate understanding of the reaction mechanisms involved in the decomposition of molecular energetic materials such as the nitro-amine FOX-7 (1,1-diamino-2,2-dinitroethylene; Scheme 1) and of the successive reactions of the radical fragments produced in these processes is imperative to predict the long-term stability (aging behavior),[1,2] explosion efficiency (performance),[3,4] and the sensitivity to heat and shock of energetic materials.[5−11] These insights are further invaluable to dispose of energetic materials safely under controlled conditions, to model the time dependence during the ignition stage of explosives, and to develop novel insensitive energetic materials.[12] The investigation of these processes along with the consecutive reactions of the transient radicals represents a fundamental challenge for experimentalists, theoreticians, and modelers[13] considering the non-equilibrium conditions under which these reactions often occur, as radicals can be born with excess kinetic and internal, i.e., rovibrational, energy and in excited electronic states.[14] This excess energy results in nonthermal equilibrium conditions so that entrance barriers (or classical activation

Scheme 1. Calculated Bond Angles (deg) and Distances (pm) of a Single Gas phase FOX-7 in Its Neutral Form[a]

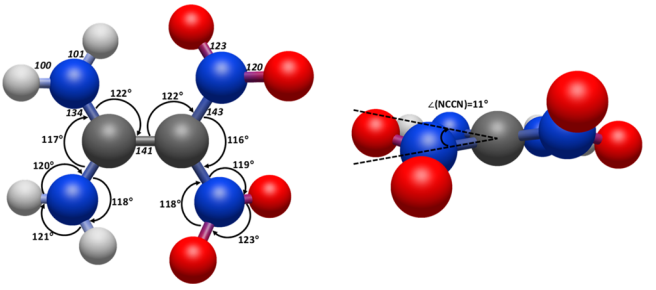

[a]The atoms of the $(H_2N)_2CC$ moiety are in a single plane with the nitrogen of one nitro group above and the other nitrogen below this plane.

Received: April 19, 2022
Revised: July 1, 2022

energies) can be overcome.[15] The decomposition of nitroamine-based molecular energetic materials is very complex. Compared to nitramine-based explosives such as RDX (1,3,5-trinitro-1,3,5-triazine), HMX (octahydro-1,3,5,7-tetranitro-1,3,5,7-tetrazocine), and CL-20 (hexanitrohexaazaisowurtzitane), which only carry nitro moieties ($-NO_2$), the incorporation of amino groups ($-NH_2$) expects more diverse decomposition pathways. Considering that FOX-7 was first synthesized in 1998,[16] experimental and computational gas phase and condensed phase studies on the decomposition of FOX-7 are sparse.

In the gas phase, experimental studies by Yuan and Bernstein[17] observed rotationally cold but vibrationally hot nitric oxide (NO). A theoretical treatment of the decomposition of FOX-7 reveals that conical intersections (CIs) are of critical importance. The S_2 state can nonradiatively decay via $(S_2/S_1)_{CI}$ and $(S_1/S_0)_{CI}$ conical intersections to lower states and might be critically involved in the nitro-to-nitrite isomerization, thus generating nitric oxide on the S_0 surface. These computations propose that the C—NH_2 bond cleavage is unlikely and nitrous acid (HONO) production on the ground state surface is energetically feasible. Computational studies by Politzer et al. at the DFT-B3P86/6-31+G(d,p) level revealed C—NO_2 and C—NH_2 bond dissociation energies of 293 and 467 kJ mol^{-1}, respectively.[18] Gindulyte et al.[19] proposed the unimolecular decomposition of FOX-7 to be initiated by a nitro-to-nitrite rearrangement via a barrier of 247 kJ mol^{-1} followed by nitric oxide (NO) loss yielding a $(H_2N)_2CC(O)NO_2$ radical. A successive hydrogen shift from the amino group to the oxygen atom of the NO_2 moiety yields $H_2N(NH)CC(O)NOOH$, which then eliminates nitrous acid (HONO). The $H_2N(NH)CCO$ cofragment may decompose to H_2NCNH along with carbon monoxide (CO), the amino radical (NH_2), and hydrogen isocyanide (HNC). This study was disputed by Zong et al. revealing that the C—NO_2 bond rupture should dominate in the temperature regime 250−3300 K whereas the nitro-to-nitrite isomerization should control the decomposition only at temperatures lower than 500 K.[20] Zong et al. discovered a third pathway initiated by a hydrogen migration from the amino group ($-NH_2$) to the oxygen atom of the nitro moiety ($-NO_2$) followed by elimination of nitrous acid (HONO). Kimmel et al. explored the role of charge transfer processes and excited states in the decomposition of FOX-7 computationally.[21] This work demonstrated that the branching ratio of two competing primary decomposition mechanisms, i.e., C—NO_2 bond fission versus nitro-to-nitrite isomerization, are affected by charge trapping and/or electronic excitation disfavoring the nitro-to-nitrite isomerization. Hydrogen atom transfer reactions were predicted to be unimportant in the decomposition of FOX-7 in the gas phase but were suggested to be of potential relevance in the condensed phase. In agreement with Politzer et al.,[18] the C—NO_2 bond was found to be substantially weaker than the C—NH_2 bond, i.e., bond energies of 280 and 503 kJ mol^{-1}, respectively. Booth and Butler[22] reinvestigated the nitro-to-nitrite isomerization computationally and also discovered a three-member cyclic intermediate. Three initial decomposition pathways were predicted. These are (i) C—NO_2 bond rupture and nitrogen dioxide (NO_2) loss, which is endoergic by 290 kJ mol^{-1}, (ii) a nitro (C—NO_2) to nitrite (C—ONO) isomerization through a barrier of 244 kJ mol^{-1}, and (iii) a hydrogen shift from the amino group to the carbon atom followed by NO_2 loss. The C—NO_2 bond energy of Turker et al.[23] of 297 kJ mol^{-1} agrees nicely with the data from Booth and Butler.[22] In addition, Ma et al. found that the crystalline environment impacts the reaction energies compared to gas phase calculations by increasing the reaction barriers because of hydrogen bonding and $\pi-\pi$ stacking.[24]

In the solid phase, experimental studies suggested a decomposition temperature of FOX-7 close to 503 K, leading eventually to water (H_2O), carbon dioxide (CO_2), hydrogen cyanide (HCN), nitrous oxide (N_2O), dinitrogen trioxide (N_2O_3), nitrogen dioxide (NO_2), nitric oxide (NO), cyanic acid (HOCN), nitrous acid (HONO), and formic acid (HCOOH).[25] Differential scanning calorimetry (DSC) and thermogravimetry (TG) supported a computationally predicted nitro-to-nitrite rearrangement followed by elimination of nitric oxide (NO). Higher order reaction products were also identified, such as isocyanic acid (HNCO), hydrogen cyanide (HCN), ammonia (NH_3), carbon dioxide (CO_2), and carbon monoxide (CO).[26] Recent laser-induced breakdown spectroscopy (LIBS) and selected ion flow tube mass spectrometry (SIFT-MS) studies[27] identified nitric oxide (NO), nitrogen dioxide (NO_2), nitrous acid (HONO), formaldehyde (H_2CO), and acetylene (C_2H_2) along with atomic nitrogen, carbon, and hydrogen as determined via UV−vis spectroscopy. Zhang et al.[28] suggest that in the condensed phase, reactive radicals like hydroxyl (OH) and nitrogen dioxide (NO_2) may undergo hydrogen abstraction with FOX-7. Gupta et al.[29] utilized time-resolved Raman spectroscopy to investigate the response of shock-compressed FOX-7. Molecular dynamics simulations for 16 FOX-7 molecules in a lattice at 3000 K revealed nitrogen dioxide (NO_2) as the result of C—NO_2 bond dissociation in the early stage of up to 10 ps converting eventually to nitrogen (N_2) and water (H_2O) within 50 ps.[30] These processes involve complex intermediates such as $C_{13}H_8N_{12}O_7$ (10 ps), $C_9H_6N_{10}O_6$ (20 ps), and $C_{10}H_8N_{10}O_9$ (30 ps), but the authors did not provide detailed chemical structures. Liu et al. explored the decomposition of FOX-7 in the condensed phase via *ab initio* molecular dynamic simulations.[31] This work revealed three initial decomposition pathways involving C—NO_2 fission and also inter- and intramolecular hydrogen atom transfer reactions, in contradiction to previous computational studies. Recent results from molecular dynamics simulations combined with experimental studies proposed that C—NO_2 cleavage represents the primary decomposition step of FOX-7.[32] A secondary reaction involves the C=O functional group formed via a three-membered cyclic transition state followed by nitric oxide (NO) elimination. The remaining cage structure loses atomic hydrogen along with amine (NH_2) radicals resulting in the formation of iminoketene (NHC=C=O). Eventually, the major decomposition products were nitrogen (N_2), ammonia (NH_3), carbon dioxide (CO_2), and diazene (H_2N_2). Exploiting photoionization, signals at m/z = 72.72, 55.81, 45.79, and 29.88 were assigned to diaminoketene ($(NH_2)_2C=C=O$), aminoketene ($NH_2CH=C=O$), nitrogen dioxide (NO_2), and nitric oxide (NO). Rashkeev et al.[33] calculated the N—O, N—H, C—NH_2, and C—NO_2 bond dissociation energies and found the C—NO_2 energy to be the lowest at 301 kJ mol^{-1}. Therefore, the authors suggested that in an α-FOX crystal, the decomposition commences with a homolytic cleavage of the C—NO_2 bond.

The aforementioned compilation suggests that no consistent picture has emerged on the decomposition mechanisms and products of FOX-7 in the solid state. Whereas molecular beam gas phase studies have yielded excellent information on the

https://doi.org/10.1021/acs.jpca.2c02696
J. Phys. Chem. A XXXX, XXX, XXX−XXX

dynamics of the decomposition of FOX-7, the decomposition of energetic materials in the solid state is more complex and is expected to deliver a greater variety of reaction intermediates and products compared to the analogous processes in the gas phase. This is because of successive reactions of the initial radical products and also the cage effect in the solid state, in which initial decomposition products—mainly radicals—react reversibly back to the original reactant molecule or to a structural isomer such as the nitro-to-nitrite isomerization in RDX.[34,35] Therefore, the decomposition of energetic materials in the solid state is expected to be more complex and can yield to a greater variety of reaction intermediates, products, and reaction mechanisms compared to the analogous processes in the gas phase under collision-less conditions. Therefore, a high-level experimental investigation of the decomposition of FOX-7 in the solid state is required.

Here, we explore experimentally the fundamental mechanisms involved in the initial decomposition phase of FOX-7 in the solid state at 5 K. These data are necessary for the energetic material community to unravel the fundamental reaction mechanisms and bond breaking processes that trigger the decomposition of energetic molecules and "switch on" the source of nonthermal radicals in the decomposition. These objectives are accomplished by photolytically triggering the decomposition of FOX-7 by pumping energy into these molecules via single wavelength ultraviolet photodissociation (UVPD) in experiments at 532 nm (2.33 eV; 225 kJ mol^{-1}) and 355 nm (3.49 eV; 337 kJ mol^{-1}) probing the n → π^* and $\pi \rightarrow \pi^*$ transitions while tracing the reactive intermediates and products formed in these processes in an ultrahigh-vacuum chamber. These excitation energies are well below the ionization energy of FOX-7 of 9.13 eV,[36] thus excluding any ion chemistry in the condensed phase. However, the selected energies are *below* (532 nm; 225 kJ mol^{-1}) and *above* (355 nm; 337 kJ mol^{-1}) the energy of the transition state involved in the nitro-to-nitrite isomerization of 244−247 kJ mol^{-1}. Thus, the choice of excitation wavelengths enables us to cover critical and major transitions and reaction barriers that populate the electronic spectrum of FOX-7. Our experimental setup incorporates highly complementary detection schemes to monitor these processes online and *in situ* in the solid state (Fourier transform infrared (FTIR), ultraviolet−visible (UV−vis) spectroscopy) by analyzing the products subliming into the gas phase via single vacuum ultraviolet (VUV) photon soft photoionization (PI) followed by a mass spectroscopic analysis of the ions in a reflectron time-of-flight mass spectrometer (ReTOF-MS). This technique identifies molecules on the basis of a correlation of their mass-to-charge ratio with their adiabatic ionization energies (IEs) and the sublimation temperature. A residual gas analyzer operating in the electron-impact mode with 70 eV electrons represents a complementary, albeit not isomer-selective analytical tool, and this unique combination reveals the fundamental, yet complex, initial dissociation processes of FOX-7. In combination with electronic structure calculations, these investigations identify the wavelength-dependent, initial decomposition products of FOX-7 in the solid state, explore local minima on the potential energy surface, and elucidate isomerization processes along with unusual reaction mechanisms involving conical intersections and bond-cleavage processes.

2. EXPERIMENTAL SECTION

2.1. Sample Preparation. FOX-7 was synthesized in house as described by Latypov et al.[37] and Astrat'ev et al.[38] with a yield of 76%. The purity of FOX-7 was checked by using NMR and elemental analysis (Supporting Information). Samples of FOX-7 were prepared by dissolving 4 mg of FOX-7 in 2.4 g of dimethyl sulfoxide (DMSO, 99.9%, Sigma-Aldrich). This 1:600 w/w solution was dispensed dropwise onto a polished silver wafer. The solution was dried under vacuum for several hours until a thin film of FOX-7 covering 1 cm^2 emerged. By using the known volume, and thus mass, dispensed onto the wafer, along with the density of solid FOX-7 (1.89 g cm^{-3}), we determined the typical thickness of the FOX-7 layers to be 2.0 ± 0.2 μm. This is consistent with weighing the silver wafer before and after the preparation of the FOX-7 film.

2.2. Experimental Setup. The experiments were conducted in an ultrahigh-vacuum (UHV) surface science chamber evacuated to base pressures of a few 10^{-10} Torr with the help of magnetically levitated turbo molecular pumps coupled to oil-free dry scroll pumps.[39,40] The FOX-7 coated, highly reflective rhodium-coated silver substrate was attached to an oxygen free high-conductivity copper (OFHC) cold-finger via indium foil. This allows for monitoring thin films on the substrates via absorption−reflection−absorption spectroscopy from the infrared (IR) to the ultraviolet−visible (UV−vis). The cold head is mounted to a closed-cycle helium refrigerator (Sumitomo Heavy Industries, RDK-415E). The substrate temperature can be selected between 5 and 300 K with the assistance of an interfaced cartridge heater and a silicon diode (Lakeshore DT-670). To remove traces of DMSO trapped within the FOX-7 crystal, the sample was cooled first to 5 K prior to heating at 1 K min^{-1} to 320 K. The complete process was monitored via a residual gas mass spectrometer that probed the subliming DMSO. At 320 K, the infrared (IR) and ultraviolet−visible (UV−vis) spectra of the FOX-7 film was recorded. Both spectrometers were aligned along the centerline with respect to the target ensuring that both the IR and the UV−vis spectra could be collected simultaneously. Briefly, a Nicolet Fourier transform infrared (FTIR) 6700 spectrometer with liquid nitrogen cooled MCTB-type detector probes the FOX-7 samples in the 11000−500 cm^{-1} region. Infrared spectroscopy is utilized to observe functional groups, identify small individual molecules, and follow the isomerization processes such as nitro-to-nitrite isomerization as the $-NO_2$ and −ONO groups hold distinct group frequencies. UV−vis spectra are recorded by a Thermo Scientific Evolution 300 spectrometer operating in the range 190−1100 nm (9091 cm^{-1}); therefore, the ranges of the FTIR and UV−vis spectrometers overlap. A detailed analysis of the recorded spectra reveals that the aforementioned heating procedure results in the presence of pure α-FOX-7 at 320 K (Results).

These samples were then recooled to 5 K, and FTIR and UV−vis spectra were recorded again prior to the photolysis revealing a hitherto unknown low-temperature phase of FOX-7 (Results). To investigate the effect of the excitation wavelength on the photolysis mechanism of FOX-7, we chose wavelengths at 532 nm (2.33 eV; 225 kJ mol^{-1}) and 355 nm (3.493 eV; 337 kJ mol^{-1}) to probe the n→ π^* and $\pi \rightarrow \pi^*$ transitions. These wavelengths were obtained by utilizing the second (532 nm) and third (355 nm) harmonics of a 30 Hz Nd:YAG laser

https://doi.org/10.1021/acs.jpca.2c02696
J. Phys. Chem. A XXXX, XXX, XXX−XXX

(Spectra Physics Quanta Ray Pro 250) while simultaneously monitoring the samples via FTIR and UV−vis spectroscopy, and the samples were irradiated for 5 h at 2.3 ± 0.5 × 10^{15} photons s^{-1} cm^{-1}. After the irradiation, the sample was annealed from 5 to 300 K at 1 K min^{-1} by using a temperature-programmed desorption scheme (TPD). The subliming molecules were recorded by using two mass spectrometric techniques. First, a quadrupole mass spectrometer (QMS) operating in residual gas analyzer mode (RGA) was less sensitive but capable of detecting any compound in sufficient quantities using 70 eV electron impact ionization (EI). Second, a reflectron time-of-flight mass spectrometer (ReTOF-MS, Jordan TOF Products, Inc.) utilizing tunable photoionization (PI) and pulsed (30 Hz) vacuum ultraviolet (VUV) photons proved to be a much more sensitive method for detecting subliming species with ionization energies (IE) less than the photon energy.

In detail, a photon energy of 10.49 eV was obtained by tripling the third harmonic of a Nd:YAG laser utilizing nonresonant four-wave mixing ($3\omega_1 = \omega_{vuv}$) by using xenon as the nonlinear medium.[41] The photon energies of 9.5 and 8.9 eV were generated by exploiting resonant difference four-wave mixing ($2\omega_1 - \omega_2 = \omega_{vuv}$) using two Nd:YAG lasers that pumped two dye lasers.[42] The resulting VUV photons were directed over the surface of the FOX-7 sample by a lithium fluoride (LiF) biconvex lens where photoionization of subliming molecules occurred. The ionized molecules were detected by the ReTOF-MS using two microchannel plates in chevron configuration. The signal was amplified with a fast preamplifier (Ortec 9305) and recorded with a multichannel scaler (MCS, FAST ComTec, MCS6A) triggered at 30 Hz (Quantum Composers, 9518). The MCS records the signal from the discriminator in 4 ns bins triggered at 30 Hz by a pulse delay generator (Quantum Composers 9518). A total of 3600 sweeps were collected per mass spectrum per 2 K increase in the temperature during the TPD phase.

3. COMPUTATIONAL DETAILS

The geometry optimization and frequency calculation of FOX-7, intermediates, transition states, and products involved in the unimolecular decomposition were carried out with dispersion-corrected density functional theory (DFT) M06-2X-D3/def2-TZVPP[43−45] in NWChem (Version 6.8.1).[46] All transition states were confirmed with the number of vibrational modes ($3N-6$ for FOX-7, intermediates, and products; $3N-7$ for transition states; N is the number of atoms) and intrinsic reaction coordinate (IRC)[47−49] calculations at the same level of theory. The potential energy of DFT-optimized structures was calculated by using the coupled-cluster method with single and double excitations and a perturbative treatment of triple excitations (CCSD(T)-F12a/cc-pVTZ-F12)[50−53] with density fitting (DF) and resolution of the identity (RI)[54] approximations in Molpro (Version 2021.2).[55,56] At the expense of slightly higher computation cost compared to CCSD(T)/cc-pVTZ,[57] the accuracy of CCSD(T)-F12a/cc-pVTZ-F12 is comparable to conventional CCSD(T) with the completed basis set (CBS)[58] level and the error of the potential energy can be as low as 0.01 eV.[53] The CCSD(T)-F12a/cc-pVTZ-F12//M06-2X-D3/def2-TZVPP + ZPE(M06-2X-D3/def2-TZVPP) method was also used to compute adiabatic ionization energies, IE, which corresponds to the energy difference between the ground vibrational levels of the cation and the neutral molecule. The isomerization barriers of N_2H_2 were calculated by using MRCI+Q/AVQZ//CASSCF(12,10)/AVQZ + ZPE(CASSCF(12,10)/AVQZ) (Figure S1).

It is important to note that the potential energy profile of gas phase FOX-7 should not be expected to reproduce the experimentally determined crystal structure of solid α-FOX-7 ($P2_1/n$, Z = 4, a = 6.9467(7) Å, b = 6.6887(9) Å, c = 11.3500(13) Å, β = 90.143(13)°).[59] From the perspective of the potential energy alone, the condensed phase environment distorts the geometry of FOX-7 from the optimal gas phase structure (i.e., increases potential energy) and stabilizes the distorted FOX-7 molecules via intermolecular interactions, mostly hydrogen bonding. Unfortunately, it is not feasible to characterize the potential energy of condensed phase α-FOX-7 at the CCSD(T)-F12a/cc-pVTZ-F12 level; therefore, the following approaches were adopted to account for the condensed phase environment in which the "distorted" crystalline α-FOX-7 absorbs the photon and the decomposition takes place. Comparison of the geometries of the gas phase FOX-7 and the distorted FOX-7 shows the changes of intramolecular bond lengths are mostly less than 10 pm, but the nitro (NO_2) groups rotate significantly: one nitro group rotates toward an in-plane position (Φ(CCNO) = 23° → 6°) and the other nitro group rotates out-of-plane (Φ(CCNO) = 23° → 33°, Figure S2). The potential energy difference between the gas phase optimal FOX-7 and the distorted α-FOX-7 molecule was quantified in Molpro with complete active-space second-order perturbation theory (CASPT2)[60,61] with the def2-TZVPP basis set using a complete active space self-consistent field with 14 active electrons and 9 active orbitals (CASSCF(14,9)).[62] Multireference methods such as CASPT2 were employed instead of a single reference method such as CCSD(T)-F12a for the distorted FOX-7 because of its multireference character. To account for the stabilizing impact introduced by the condensed phase environment, small clusters of molecules up to octamers were constructed according to the crystal structure of α-FOX-7) and its potential energy was computed at the M06-2X-D3/def2-TZVPP level of theory. As shown in the Results, most of the α-FOX-7 molecules in the thin film remained intact during the initial decomposition process triggered by the laser. Therefore, only the center molecule in the small cluster adapts a different configuration while neighboring molecules remain intact.

Because FOX-7 exists in the singlet state and because of the spin-forbidden rule of transition, intersystem crossing (ISC) would have taken place if only one of the two decomposition products is in the triplet state, e.g., atomic or molecular oxygen. To locate the potential geometrical regions that are relevant to ISC, the lowest lying singlet and triplet pathways involving triplet atomic and molecular oxygen were recalculated at the CASSCF(14,9)/def2-TZVPP level of theory with a Lagrange multiplier[63] to search for the minima on the seam of crossing (MSX). The potential energies of the optimized MSXs were further calculated at the CASPT2/def2-TZVPP level.

4. RESULTS

4.1. Infrared Spectroscopy. Several phases of FOX-7 denoted as α to ζ have been characterized, among them α-FOX-7, which is stable at temperatures below 389 K.[59,64−67] Single crystal X-ray diffraction studies reveal a monoclinic structure with four formula units per unit cell. As a typical push−pull ethylene (Scheme 1), the carbon−carbon bond in α-FOX-7 is 145 pm long, which is shorter than a carbon−carbon single bond in ethane (154 pm), but longer than a

https://doi.org/10.1021/acs.jpca.2c02696
J. Phys. Chem. A XXXX, XXX, XXX−XXX

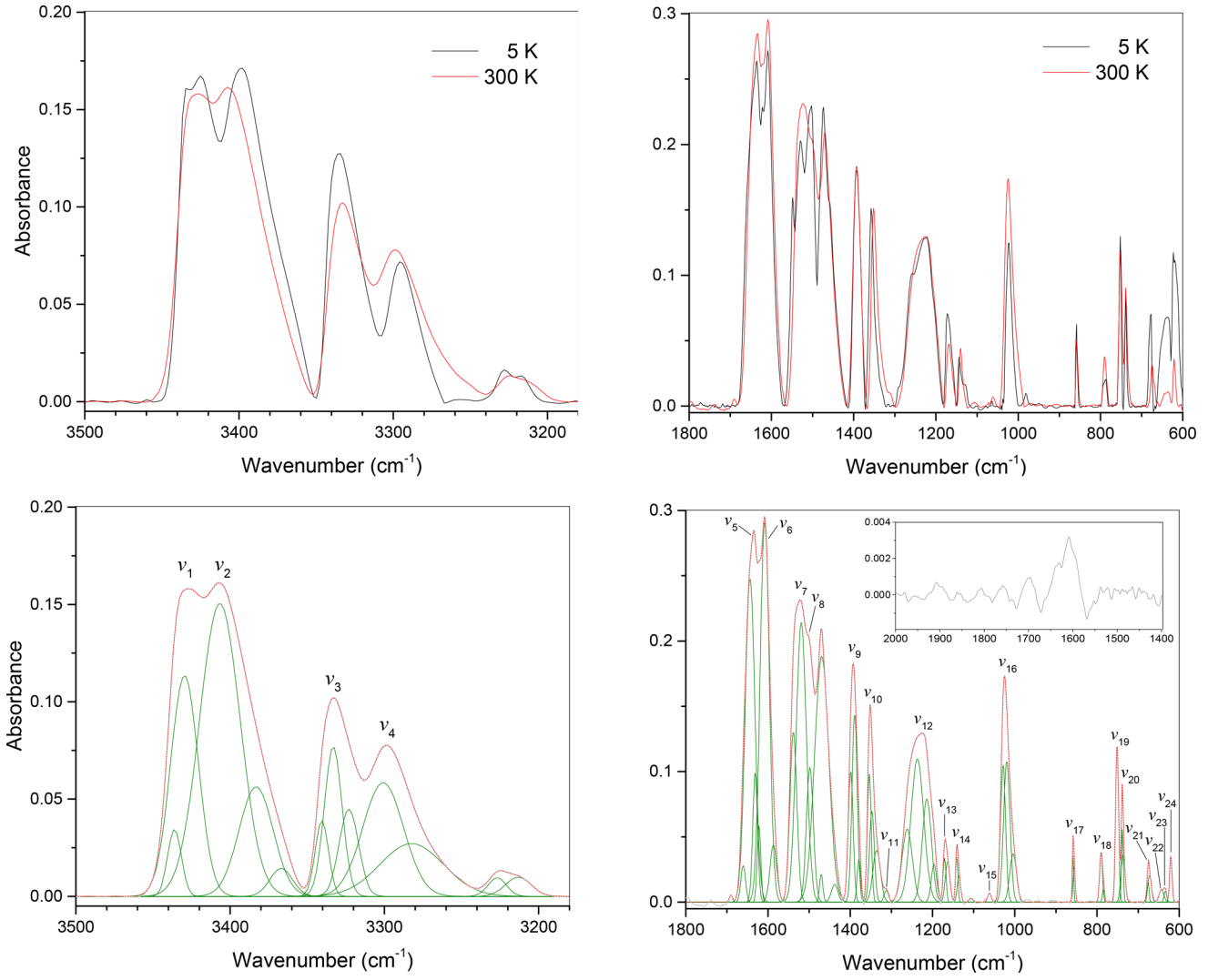

Figure 1. Top: Infrared spectra of FOX-7 taken at 300 K (red) and 5 K (black). Bottom: Deconvoluted infrared spectra of FOX-7 taken at 300 K with peak assignments (see Table 1). Inset: Difference spectrum between FOX-7 spectra taken before and after irradiation with 355 nm showing the −ONO stretching mode.

carbon−carbon double bond in ethylene (134 pm).[68] The electron-pushing amino (NH_2) and electron-pulling nitro (NO_2) groups cause not only a highly polar carbon−carbon bond but also intra- and intermolecular hydrogen bonds. The molecular configuration of the carbon atoms and the amino groups is essentially planar, while the nitrogen atoms of the nitro group are out-of-plane with one nitrogen residing above and the other below the plane defined by the carbon atoms and amino groups. Two intramolecular hydrogen bonds are present between the hydrogen atoms of the amino group and the oxygen atom of the nitro group (Scheme 1). This results in a local symmetry of the FOX-7 molecule with a C_2 rotation axis through both carbon atoms. The molecular packing consists of wave-shaped layers with extensive intermolecular hydrogen bonding within the layers with each oxygen atom of the nitro group taking part in two hydrogen bonds and van der Waals forces between the layers.

Because the decomposition mechanisms of molecular energetic materials may depend on the phase, it is important to define the phase of FOX-7 in the present study. Here, the infrared spectrum of FOX-7 was recorded under UHV conditions at 300 K (Figure 1, Figure S3, Table 1). Among the computed 36 fundamental modes,[69,70] ν_{25}−ν_{36} are below the cutoff of the infrared detector; hence, only ν_1−ν_{24} are discussed.[71] In the high-energy range from 3500 to 3200 cm^{-1}, the spectrum is dominated by the symmetric and asymmetric stretching modes of the NH_2 functional group (ν_1−ν_4). The symmetric stretching between the carbon and amine groups (ν_5) could be observed at 1633 cm^{-1}, while the scissoring modes of the NH_2 functional group (ν_6−ν_7) are visible at about half of the wavenumbers observed for the stretching modes from 1608 to 1523 cm^{-1}. Stretching of the C═C bond is assigned to ν_8 and ν_9 at 1503 and 1392 cm^{-1} followed by stretching of the NO_2 functional group at 1352 cm^{-1} (ν_{10}, asymmetric) and 1169−1141 cm^{-1} (ν_{13}−ν_{14}, symmetric). Rocking of the amine moiety covers a broad region from 1312 to 1025 cm^{-1} and can contribute to ν_{11}−ν_{16}. Carbon−nitrogen stretching occurs from 1312 to 1221 cm^{-1} with the symmetric stretch of C—NO_2 assigned to ν_{11} (1312 cm^{-1}) and the asymmetric stretch at 1221 cm^{-1} (ν_{12}). The scissoring modes of the NO_2 moiety (ν_{17}, ν_{19}) also emerge at about half of the frequency compared to the asymmetric stretching mode. Lower wavenumber wagging, rocking, and twisting modes (ν_{18}, ν_{20}−ν_{24}) complement the spectrum. A comparison of these

https://doi.org/10.1021/acs.jpca.2c02696
J. Phys. Chem. A XXXX, XXX, XXX−XXX

Table 1. Experimental Infrared Band Positions of FOX-7 Compared to Calculated Values

mode[a]	this work[b] (cm^{-1})	this work[c] (cm^{-1})	calcd[d] (cm^{-1})	calcd[e] (cm^{-1})	expt[f] (cm^{-1})	assignment[g]
1	3425		3433	3450	3425	$\nu_{as}(NH_2)$
2	3406	3402	3418	3424	3405	$\nu_{as}(NH_2)$
3	3333	3329	3321	3334	3333	$\nu_{s}(NH_2)$
4	3298	3295	3288	3293	3299	$\nu_{s}(NH_2)$
	3225	3226				$\nu_5 + \nu_6$[h]
	3212					$2\nu_6$[h]
5	1633	1632	1603	1624	1630	$\nu_{s}(C-NH_2)$
	1622	1622				$\nu_{16} + \nu_{24}$[h]
6	1608	1605	1562	1599	1606	$\delta_{s}(NH_2)$
7	1523	1520	1497	1519	1528	$\delta_{s}(NH_2)$
8	1503		1480	1493	1506	$\nu(C-C)$
	1470	1470			1464, 1481	$\nu_{17} + \nu_{24}$[f]
9	1392	1390	1398	1411	1386	$\nu(C-C)$
10	1352	1350	1321	1339	1343	$\nu_{as}(NO_2)$
	1337				1336	$\nu_{17} + \nu_{27}$ (481 cm^{-1})[f]
11	1312		1300	1315	1311	$\rho(NH_2)$, $\nu_{s}(C-NO_2)$[e]
12	1221	1212	1190	1201	1208	$\rho(NH_2)$, $\nu_{as}(C-NO_2)$[e]
13	1169	1166	1141	1156	1165	$\rho(NH_2)$, $\nu_{s}(NO_2)$
14	1141	1140	1106	1119	1142	$\rho(NH_2)$, $\nu_{s}(NO_2)$
15	1063		1050	1084	1070	$\rho(NH_2)$
16	1025	1022	1006	1063	1024	$\rho(NH_2)$
17	858	857	833	843	856	$\delta_{s}(NO_2)$
18	790	789	797	821	789	$\tau(NH_2)$
19	751	749	766	775	749	$\delta_{s}(NO_2)$
20	739	738	735	741	737	$\delta(C-NO_2)$, $\tau(NH_2)$
21	674	673	715	723		$\delta(C-NO_2)$, $\tau(NH_2)$
22	644		668	695		$\omega(NH_2)$
23	635	636	658	681		$\tau(NH_2)$
24	620	617	633	676	622	$\tau(NH_2)$, $\delta_{s}(NH_2)$

[a]Normal mode designations based on ref 69. [b]Solid sample under UHV conditions. [c]Powdered sample at ambient conditions. [d]Calculated values from ref 69. [e]Calculated values from ref 70. [f]Experimental values from ref 71. [g]Assignments from ref 69. [h]Assigned in this work.

features with the infrared spectra of distinct phases of FOX-7 reveals that FOX-7 exists in the monoclinic α phase, which is stable at temperatures below 389 K (Table 1).[59,64−67] Infrared spectra of the freshly prepared FOX-7 and results of differential thermal analysis are presented in Figures S6 and S7.

When the α-FOX-7 phase was cooled to 5 K, changes in the infrared spectrum were visible (Figures 1 and 2). The most noticeable changes arose in the high-wavenumber range from 3500 to 3200 cm^{-1}, which covers the asymmetric and asymmetric stretches of the amino group. For $\nu_1-\nu_2$ and $\nu_3-\nu_4$, the pairs of fundamentals reveal an enhanced splitting and pronounced doublet upon lowering the temperature to 5 K, which gradually emerged at, e.g., 3412 cm^{-1}. This is correlated with a rapid change of structure of the ν_1 band at 3430 cm^{-1} from 190 to 200 K. During this process, the ν_2 mode is blue-shifted from 3398 cm^{-1} (300 K) to 3408 cm^{-1} (5 K). Also, the scissoring modes of the amino group reveal a pronounced doublet as the temperature drops to 5 K, in particular for the ν_7 mode. In addition, several distinct peaks appear at low temperatures that are not in the 300 K α phase of FOX-7 (Figure 2). These bands, in particular those at 980, 1125, 1292, and 1548 cm^{-1}, gradually decline, beginning between 25 and 35 K as the low-temperature ice is heated and are largely absent at 200 K, indicating that the low-temperature phase has returned to the 300 K presentation of α-FOX-7. It shall be highlighted that the changes in the infrared spectra cannot be associated with any known higher temperature phases of FOX-7 ($\beta-\zeta$).[72] Because all bands of α-FOX-7 are present at 5 K along with the aforementioned spectroscopic modifications, we may conclude that α-FOX-7 undergoes low-temperature changes at 190 to 200 K, which we designate α'-FOX-7. This modification is reversible with α'-FOX-7 returning to α-FOX-7 upon heating from 5 to 300 K as probed infrared spectroscopically. Because all absorption bands of α-FOX-7 at 300 K also appear at 5 K, the experimentally and computationally determined phase characteristics of α-FOX-7 serve as a suitable analogue for its low-temperature α'-FOX-7 phase.

4.2. UV−Vis Spectroscopy. To the best of our knowledge, published experimental UV−vis spectra of α-FOX-7 in the condensed phase do not exist. Here, we obtained a UV−vis spectrum of α-FOX-7 by averaging the spectra of eight distinct samples at 300 K (Figure 3). This spectrum reveals a distinct absorption maximum at 395 nm that is accompanied by a shoulder at 530 nm. A broad absorption from 850 to 1100 nm (11760 to 9090 cm^{-1}) is apparent in the near-infrared regime of the electromagnetic spectrum. This broad feature could be linked to combination bands and/or overtones of the symmetric and antisymmetric stretches of the amino group ($\nu_1-\nu_4$),requiring at least three quanta. Note that the UV−vis spectrum does not change once the sample is cooled from 300 to 5 K. Compared to the spectrum of α-FOX-7, spectra of FOX-7 taken in solution reveal significant differences. Šimkova et al. explored the UV−vis spectra of FOX-7 in polar and nonpolar solvents.[73] The spectra propose an equilibrium between the traditional olefinic structure and the zwitterionic

https://doi.org/10.1021/acs.jpca.2c02696
J. Phys. Chem. A XXXX, XXX, XXX−XXX

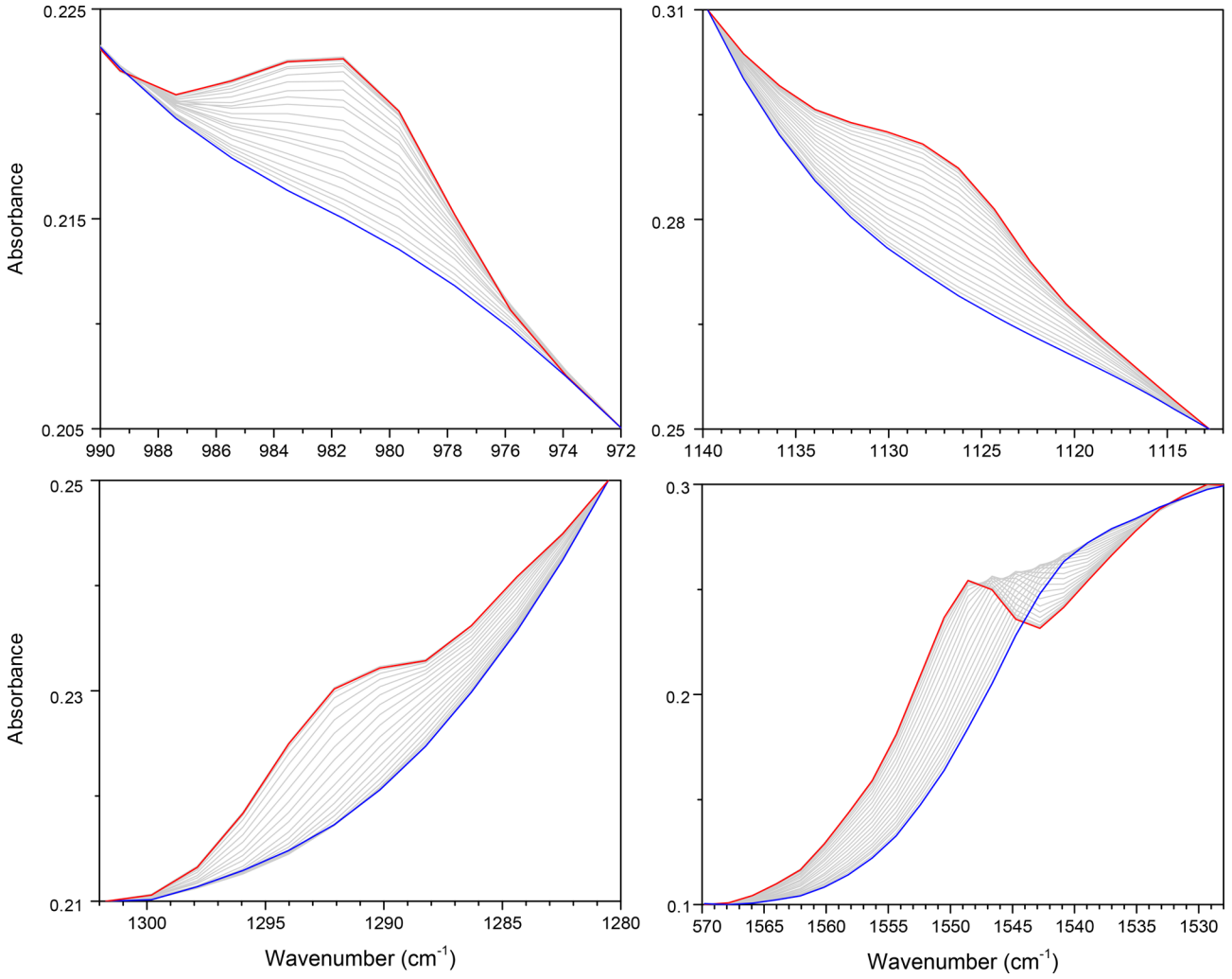

Figure 2. Temperature-dependent changes upon cooling the α-FOX-7 to 5 K associated with the following four fundamentals: ν_{16} (top left), ν_{14} (top right), ν_{12} (bottom left), ν_7 (bottom right). The red spectra were recorded at 5 K, the blue spectra were recorded at 205 K, and the gray spectra were taken in steps of 10 K.

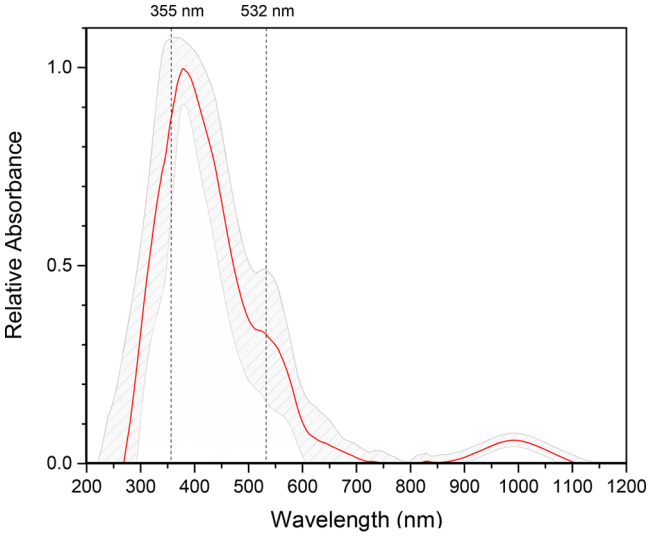

Figure 3. UV−vis spectrum of α-FOX-7 recorded at 300 K in the UHV chamber. The spectrum was obtained by averaging the spectra of eight distinct samples (red) and includes error bars (gray). The photolysis wavelengths, 355 and 532 nm, are labeled.

form (Figure S4),as evident from absorptions close to 280 and 350 nm, respectively. The olefinic structure dominates in weakly polar solvents (dichloromethane, CH_2Cl_2; acetonitrile, CH_3CN), whereas the zwitterionic structure is red-shifted to 350 nm and pronounced in polar solvents (dimethyl sulfoxide (DMSO), CH_3SOCH_3; alcohols, ROH). The latter form of FOX-7 suggests the presence of an anionic moiety formed by charge separation, i.e., the zwitterionic form of FOX-7.

4.3. Photoionization (PI) Reflectron Time-of-Flight (ReTOF) Spectroscopy. Single photon ionization (PI) reflectron time-of-flight mass spectrometry (Re-TOF-MS) represents a sensitive method to detect selectively the photodecomposition products of the FOX-7 isomer in the temperature-programmed desorption (TPD) phase from 5 to 300 K upon sublimation. This is achieved by correlating the mass-to-charge (m/z) ratios of the products with ions recorded at different photon energies (Figure 4). As the first step, the subliming molecules of the photolyzed samples (at 532 and 355 nm) were ionized with 10.49 eV photons. For the 532 nm photolyzed sample, no products could be detected. However, for the sample photolyzed at 355 nm, ion counts were detected at m/z = 30. The corresponding TPD profile is shown in Figure 5. The signal at m/z = 30 could be linked to nitric oxide

https://doi.org/10.1021/acs.jpca.2c02696
J. Phys. Chem. A XXXX, XXX, XXX−XXX

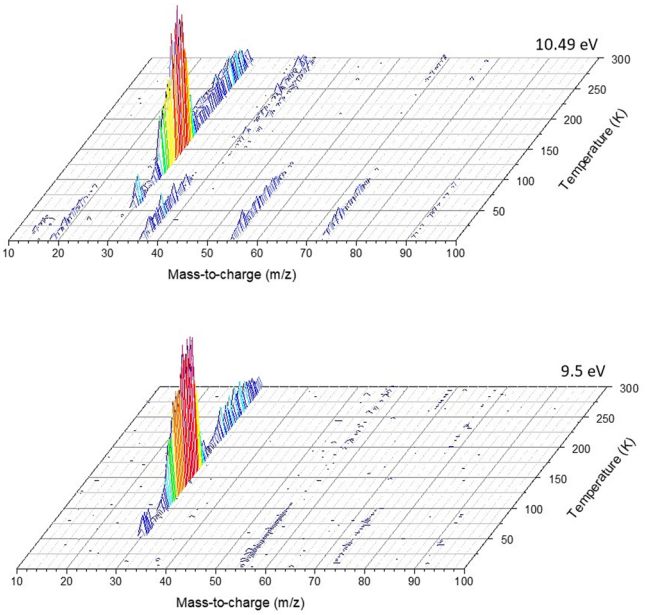

Figure 4. ReTOF temperature-programmed desorption (TPD) profiles for m/z = 10 to m/z = 100 of FOX-7 irradiated with 355 nm using 10.49 and 9.5 eV photoionization energy. No signal was observed at a photoionization energy of 8.9 eV.

(NO; IE = 9.26 ± 0.01 eV) and/or three isomers of N_2H_2: *trans*-diazene (IE = 9.61 ± 0.01 eV; HNNH), *cis*-diazene (IE = 9.64 ± 0.01 eV; HNNH), and isodiazene (IE = 8.66 ± 0.01 eV; NNH_2) (Figure S5). To discriminate these species, the photoionizing energy was lowered to 9.5 eV. This energy allows photoionization of nitric oxide (NO; IE = 9.26 ± 0.01 eV), but it is below the ionization energies of *trans*- and *cis*-diazene (IE = 9.61 ± 0.01 eV; IE = 9.64 ± 0.01). The TPD profile recorded at 9.5 eV is essentially identical to the profile collected at 10.49 eV (Figure 5). This indicates that the signal at m/z = 30 does not originate from *trans*- and/or *cis*-diazene. The photon energy was reduced further to 8.9 eV, which can ionize only isodiazene (IE = 8.66 ± 0.01 eV; NNH_2) but not nitric oxide (NO; IE = 9.26 ± 0.01 eV). The TPD profile at 8.9 eV is essentially flat and does not show any signal above the noise level. Therefore, we can conclude that in the photolysis of FOX-7 at 355 nm, only nitric oxide (NO) is formed, but no N_2H_2 isomers.

4.4. Residual Gas Analyzer. Figure 5 also shows the TPD profile collected with the residual gas analyzer (RGA) at 70 eV electron impact ionization. The signal-to-noise ratio is much worse compared to the photoionization studies at 10.49 eV; however, the TPD profile recorded with the RGA shows the same maximum at 150 K and ranges also from about 100 to 180 K. Besides signal at m/z = 30, the only observable signal above background level was m/z = 32 (Figure 6) along with an associated m/z = 16 signal. This could arise from hydrazine (N_2H_4, IE = 8.1 eV) and/or molecular oxygen (O_2, IE = 12.07 eV). Because the TPD profiles recorded at photon energies of 10.49, 9.5, and 8.9 eV do not show any signal at m/z = 32, we can conclude that the signal at m/z = 32 must be linked to molecular oxygen (O_2). Further confirmation was achieved by comparing the experimental ratio of m/z = 32 to m/z = 16 of 7.5 ± 0.2:1 to the ratio obtained by introducing pure molecular oxygen to the mass spectrometer, which produced the same m/z = 32 to m/z = 16 ratio with m/z = 16 formed through

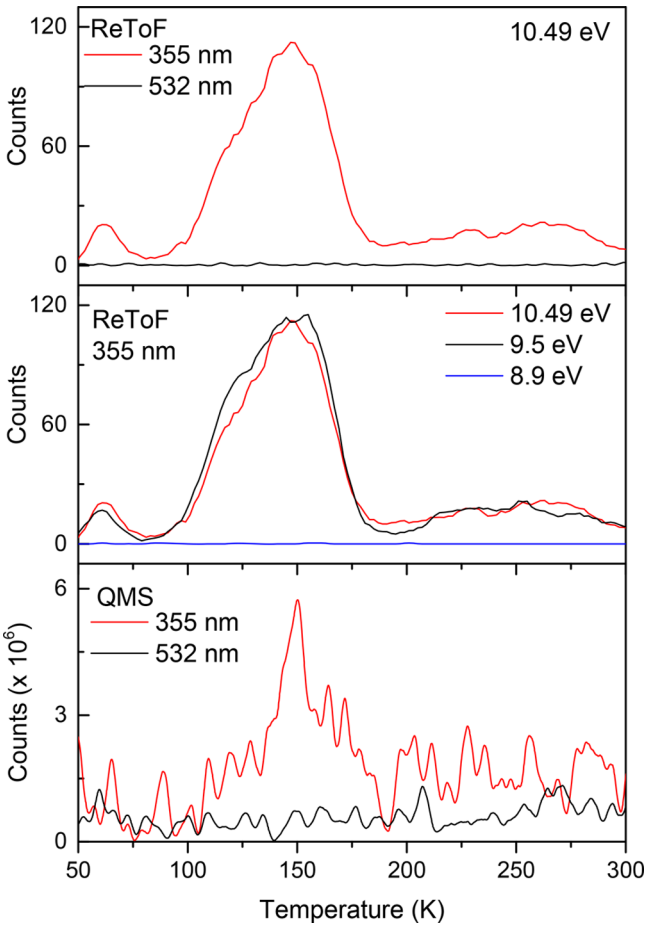

Figure 5. Temperature-programmed desorption profiles of irradiated FOX-7 tracing m/z = 30. Top: TPD profiles using 10.49 eV photoionization taken after irradiation with 355 nm (red) and 532 nm (black) photons. Center: TPD profiles taken after irradiation with 355 nm photons using photoionization energies of 10.49 eV (red), 9.5 eV (black), and 8.9 eV (blue). Bottom: QMS profiles taken after irradiation with 355 nm (red) and 532 nm (black) photons.

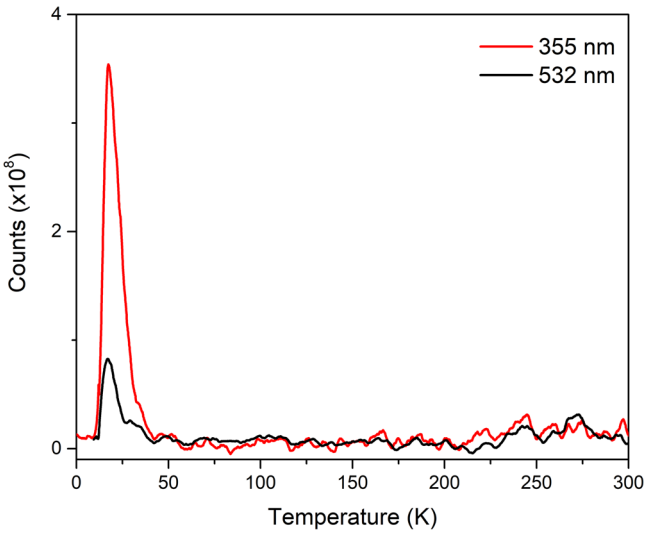

Figure 6. Temperature-programmed desorption profiles of FOX-7 irradiated at 355 nm (red) and 532 nm (black) monitoring m/z = 32 using a quadrupole mass spectrometer (QMS) as a residual as analyzer (RGA).

https://doi.org/10.1021/acs.jpca.2c02696
J. Phys. Chem. A XXXX, XXX, XXX−XXX

dissociative electron impact ionization of molecular oxygen and confirmed the assignment of molecular oxygen to m/z = 32. This signal is clearly enhanced for the sample photolyzed at 355 nm compared to 532 nm. Accounting for the photon flux, the ratio of the integrated intensities of the ion counts at m/z = 32 is 4.3 ± 0.3:1. A comparison of the molecular oxygen to nitric oxide signals, when corrected for their ionization cross-sections of 2.441 and 2.807 Å^2 at 70 eV electron impact energy,[74] shows that the signal for molecular oxygen is 700 ± 100 times larger than the signal for nitric oxide.

5. DISCUSSION

We are merging our experimental data with results from electronic structure calculations to reveal likely decomposition and reaction mechanisms of FOX-7 exposed to 532 nm (2.33 eV; 225 kJ mol^{-1}) and 355 nm (3.49 eV; 337 kJ mol^{-1}) photons. The experimental findings are summarized in Table 2.

Table 2. Comparison between the Species Detected in the Experiment and the Species Predicted from the Computation of FOX-7 Decomposition in the Gas and Condensed Phases

	experiment		computation prediction			
	532 nm	355 nm	532 nm	355 nm	532 nm	355 nm
species	224.9 kJ mol^{-1}	337.0 kJ mol^{-1}	gas phase		condensed phase	
i1/**i2**	no	yes	no	yes	yes	yes
i3	no	no	yes	yes	no	no
NO_2 + products	no	no	yes	yes	no	yes
NO + **p1**	no	yes	no	yes	yes	yes
NH_2 + **p3**	no	no	no	no	no	no
O_2 + products	yes	yes	no	no	yes	yes

First, upon photolysis, the only new signal observable via infrared spectroscopy emerged at 1610 cm^{-1}, which can be linked to a nitrite moiety (−ONO) connected to a carbon atom.[75−80] This absorption is only visible for the sample photolyzed at 355 nm. No changes are observed in the UV−vis spectra recorded before and after the photolysis at 355 or 532 nm. This is not surprising considering the weak changes in the infrared spectra (Figure 1) along with the less sensitive UV−vis detection technique. Second, molecular oxygen (O_2) was detected in the samples photolyzed at 355 and 532 nm at a ratio of 4.3 ± 0.3:1, whereas nitric oxide (NO) was only observed in the samples photolyzed at 355 nm. N_2H_2 isomers were not detected.

The key decomposition pathways of a single gas phase FOX-7 molecule are depicted in Figure 7. In the gas phase, FOX-7 can undergo decomposition via C—NO_2 bond rupture in an endothermic process (+300 kJ mol^{-1}), leading to the $(H_2N)_2CC(NO_2)$ radical (**i4**) plus nitrogen dioxide (NO_2). These data correlate nicely with previous bond dissociation energies ranging from 280 to 297 kJ mol^{-1}.[18,21−23] In the matrix, **i4** and nitrogen dioxide (NO_2) could recombine to form the nitrite isomer of FOX-7, $(H_2N)_2CC(NO_2)(ONO)$ (**i1**). The overall reaction energy between FOX-7 and its nitrite isomer (**i1**) is −18 kJ mol^{-1}. Alternatively, **i1** could be formed by a nitro-to-nitrite isomerization via a single transition state located +273 kJ mol^{-1} above FOX-7. The barrier height is in good agreement with previous studies of 244 to 247 kJ mol^{-1}.[19,22] Subsequently, **i1** can then either undergo a nitric oxide (NO) loss forming the $(H_2N)_2CC(O)NO_2$ radical (**p1**) and nitric oxide (NO) or form a transition state of +35 kJ mol^{-1} to isomerize to **i2** before forming **p1** and nitric oxide (NO). The overall reaction between FOX-7 and **p1** + NO is slightly exoergic by −15 kJ mol^{-1}. FOX-7 can also decompose through amino radical (NH_2) ejection to form $H_2NCC(NO_2)_2$ (**p3**). This decomposition is endoergic by +461 kJ mol^{-1}, which aligns with previous studies that range between 467 and 503 kJ mol^{-1}.[18,21] In addition, a hydrogen atom in FOX-7 could shift from the amino group to a carbon atom via a barrier of 203 kJ mol^{-1}, leading to intermediate **i3**, which can undergo a C—N bond rupture to form the $H_2N(HN)CCH(NO_2)$ radical (**p2**) and nitrogen dioxide (NO_2). Here we note that the $(H_2N)_2CC(NO_2)$ radical (**i4**) could isomerize to the $H_2N(HN)CCH(NO_2)$ radical (**p2**) via a hydrogen-shift transition state of 110 kJ mol^{-1} above **i4**, with **p2** being the more stable isomer by 101 kJ mol^{-1}.

In addition to the aforementioned pathways that could potentially form nitric oxide (NO) (with **p1**), the amino radical (NH_2) (with **p3**), and nitrogen dioxide (NO_2) (with **i4** and/or **p2**), the residual gas analyzer also detected the formation of molecular oxygen (O_2). Herein, we also explore computationally the potential pathways of molecular oxygen (O_2) formation in Figure 7. Molecular oxygen ($O_2(X\ ^3\Sigma_g^-)$) along with $(H_2N)_2CC(NO)_2$ (**p4**) can be formed by bonding two oxygen atoms from two adjacent nitro groups; this pathway is endoergic by 204 kJ mol^{-1}. In the gas phase, FOX-7 exists in the singlet ground state, and thus the formation of triplet $O_2(X\ ^3\Sigma_g^-)$ and singlet $(H_2N)_2CC(NO)_2$ (**p4**) must involve intersystem crossing (ISC). The minimum on the seam of crossing (**MSX-1**) is found to be 381 kJ mol^{-1} above FOX-7. Triplet atomic oxygen ($O(^3P)$) along with singlet $(H_2N)_2CC(NO)NO_2$ (**i5** and **p5**) could also be formed as a result of the N—O bond rupture and the endoergicities of these reactions are 346 and 344 kJ mol^{-1}, respectively. For the same reason, the formation of $O(^3P)$ involves intersystem crossings and the corresponding MSXs are located at 385 kJ mol^{-1} (**MSX-3**, leading to **i5**) and 337 kJ mol^{-1} (**MSX-2**, leading to **p5**) above FOX-7. In such processes, molecular oxygen (O_2) could also be formed as a result of combining two oxygen atoms trapped by the encapsulated environment in the crystalline solid.

Several dominating pathways identified computationally correlate with the experimental data (Table 2). First, the potential energy profile confirms the infrared spectroscopic detection that the 335 nm (337 kJ mol^{-1}) photons, and not the 532 nm (225 kJ mol^{-1}) photons, have sufficient energy to form **i1** and/or **i2** through either nitro-to-nitrite isomerization or the recombination between the $(H_2N)_2CC(NO_2)$ radical (**i4**) and nitrogen dioxide (NO_2). The fact that no nitrogen dioxide (NO_2; IE = 9.59 eV) was observed in the TPD data suggests that the latter (**i4** + NO_2) reacts back to the reactant in the matrix and/or forms intermediate **i1**/**i2**. Second, the computed barrier height (273 kJ mol^{-1}) of forming **i1**/**i2** also correlates well with the detection of **p1** + NO products only for 355 nm photolysis (337 kJ mol^{-1}) and not 532 nm (225 kJ mol^{-1}) photolysis. Finally, although observed by Jiang et al.,[32] the nitrogen-containing decomposition products such as ammonia (NH_3), diazene (N_2H_2), or molecular nitrogen (N_2) were not observed in the present study. The formation of these molecules is initiated by a carbon−nitrogen cleavage of the C-NH_2 moiety, e.g., forming **p3** and the amino radical (NH_2).

https://doi.org/10.1021/acs.jpca.2c02696
J. Phys. Chem. A XXXX, XXX, XXX−XXX

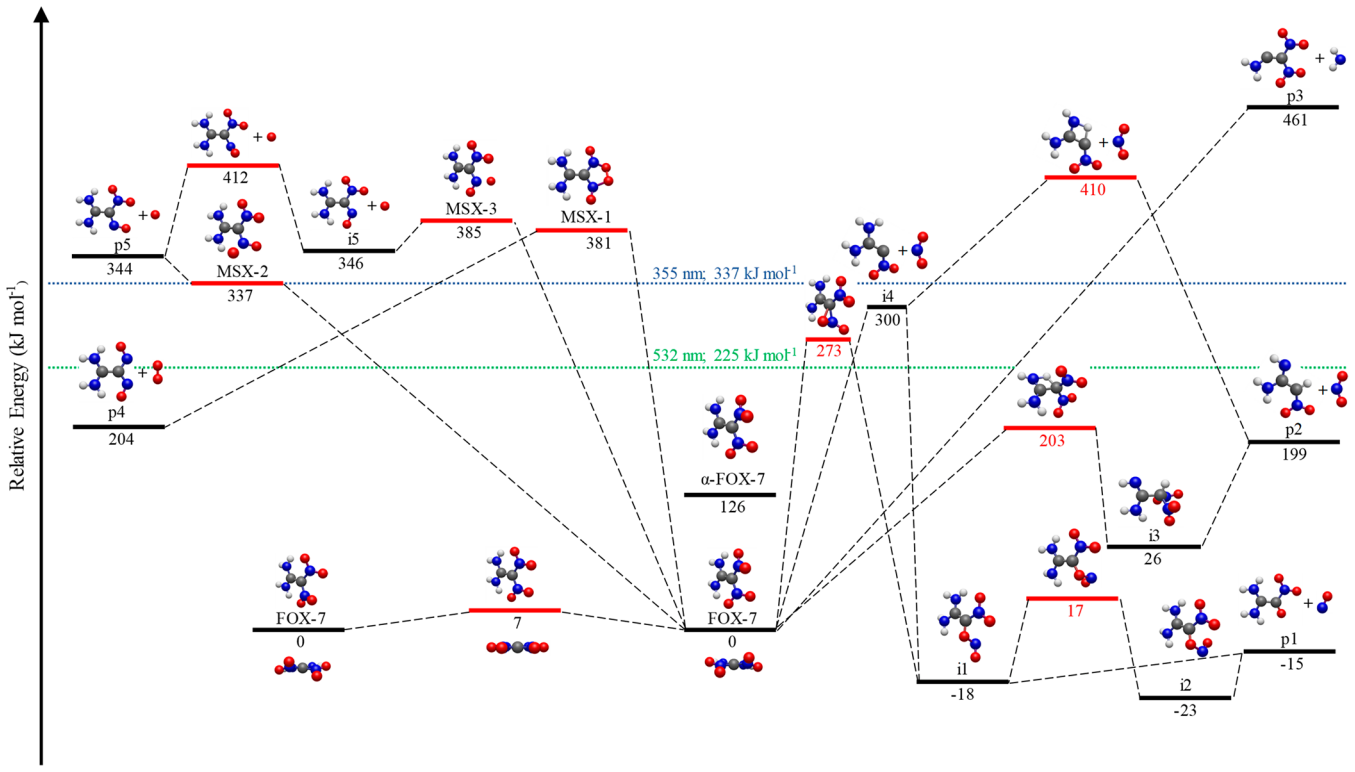

Figure 7. Gas phase potential energy profile calculated at the CCSD(T)-F12/VTZ-F12//M06-2X-D3/def2-TZVPP + ZPE(M06-2X-D3/def2-TZVPP) level of theory, revealing decomposition pathways of FOX-7 toward the formation of NO, NO_2, and NH_2 on the right side. The gas phase potential energy profile calculated at the CASPT2/def2-TZVPP//CASSCF/def2-TZVPP + ZPE(CASSCF/def2-TZVPP) level of theory, revealing decomposition pathways of FOX-7 toward the formation of oxygen ($O(^3P)$) and molecular oxygen ($O_2(X\ ^3\Sigma_g^-)$) is shown on the left side. Minima on the seam of crossing (MSX) connecting the singlet and triplet manifolds, as well as transition states, are colored in red. The relative potential energy (CASPT2/def2-TZVPP//CASSCF/def2-TZVPP + ZPE(CASSCF/def2-TZVPP)) of the gas phase FOX-7 molecule taking the structure of molecules found in the α-FOX-7 crystal is also shown. The dashed lines indicate the energy of the photons used.

According to the potential energy profile, the energy required for this process (461 kJ mol^{-1}) is energetically inaccessible through a single photon process of 355 nm (337 kJ mol^{-1}) or 532 nm (225 kJ mol^{-1}).

In spite of the aforementioned agreements between experiments and computations, it is important to note that two discrepancies remain. The first involves the formation of **p2** + NO_2. Although energetically inaccessible via the **i4** + NO_2 → **p2** + NO_2 pathway, an alternative pathway, FOX-7 → **i3** → **p2** + NO_2, should be accessible by both the 355 nm (337 kJ mol^{-1}) and 532 nm (225 kJ mol^{-1}) photons as this pathway must only overcome a 203 kJ mol^{-1} transition state. Given that the experiment failed to detect the intermediate **i3** (Table S1) or nitrogen dioxide (NO_2), the FOX-7 → **i3** → **p2** + NO_2 pathway is blocked in spite of being the most energetically accessible pathway found in the gas phase potential energy surface (Figure 7). Second, although three pathways of forming molecular oxygen (including those forming $O(^3P)$) have been characterized in Figure 7, not one of them is energetically accessible, i.e., **MSX-1**, 381 kJ mol^{-1}; **MSX-3**, 385 kJ mol^{-1}; **MSX-2**, 337 kJ mol^{-1}, by the 355 nm (337 kJ mol^{-1}) or 532 nm (225 kJ mol^{-1}) photons. However, the experiments detected the formation of molecular oxygen even with the lower energy 532 nm photon. These discrepancies indicate that the gas phase calculations only partially describe the condensed phase decomposition of FOX-7, and the encapsulated environment plays a key role in controlling the reactivity of some reaction pathways.

We emphasize that in the experiment, the photons irradiate crystalline α-FOX-7, which has a configuration that is distorted from the optimal structure found in the gas phase. To determine the electronic potential energy difference (ΔE_1) between a gas phase molecule of FOX-7 and an isolated molecule in α-FOX-7 configuration, CASPT2/def2-TZVPP was employed and computed ΔE_1 = 126 kJ mol^{-1}. However, intermolecular interactions, such as hydrogen bonds between the oxygen atoms and the hydrogen atoms of a neighboring molecule, stabilize the α-FOX-7 molecules and thus decrease the potential energy by ΔE_2. Characterizing ΔE_2 accurately is challenging as the size of the α-FOX-7 molecule cluster needs to be balanced with the accuracy of the quantum chemistry methods (M06-2X-D3/def2-TZVPP). As an example, the transition state between FOX-7 and **i1** (herein **TS1**) is employed to explore the impact of the size of the molecular cluster on how accurately it represents the decomposition of a α-FOX-7 molecule. As shown in Figure 8, the first solvation shell (three layers of α-FOX-7 molecules) is considered to simulate the encapsulated environment. First, 18 different dimers of FOX-7 molecules were constructed according to the crystal structure of α-FOX-7. As shown, these dimers contain all possible interactions between the central molecule and its neighboring molecules found in the crystal. For each dimer, the central molecule is changed to the **TS1** configuration while the neighbor molecule remains unchanged, as experiments indicate that most of the FOX-7 molecules remain intact during the decomposition process. The energy of the **TS1**/α-FOX-7 dimer is compared to the original α-FOX-7/α-FOX-7

https://doi.org/10.1021/acs.jpca.2c02696
J. Phys. Chem. A XXXX, XXX, XXX−XXX

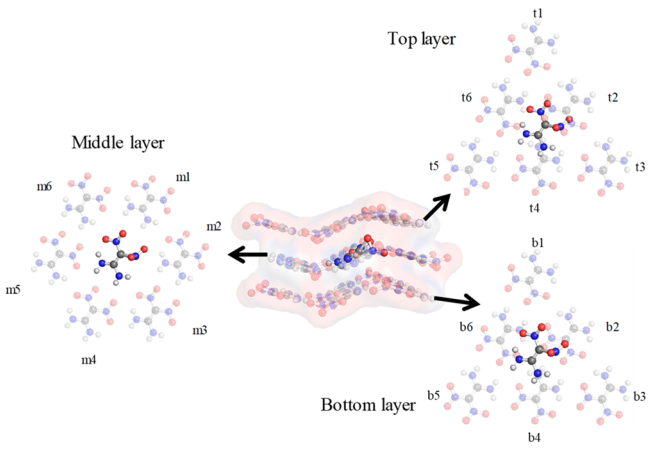

Figure 8. Demonstration of the first solvation shell of α-FOX-7. Each center molecule is surrounded by 18 α-FOX-7 molecules. The dimers are constructed with the center molecule and one neighboring molecule.

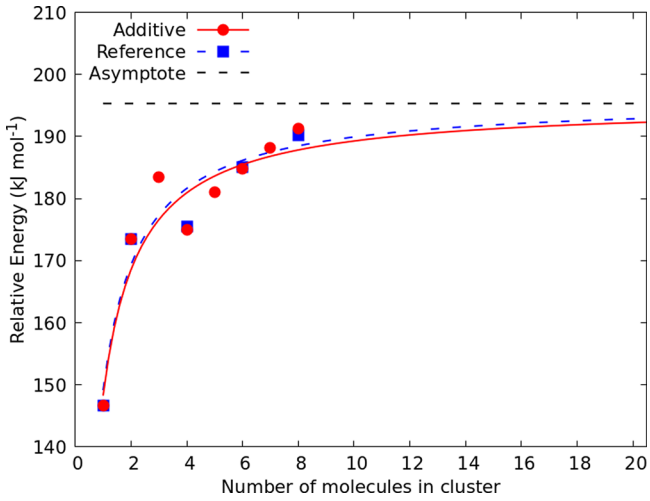

Figure 9. Example using the transition state between α-FOX-7 and **i1** (**TS1**) demonstrating the summation of energy shifts induced from neighboring molecules (additive, red). This is a good approximation of the energy shift induced from a small molecular cluster (reference, blue). Both curves approach an asymptote at 196 ± 4 kJ mol^{-1}.

dimer to assess the barrier of **TS1** in the presence of one neighboring α-FOX-7 molecule, and the results are summarized in Table 3. Compared to the barrier height of the **TS1** along, when a neighboring α-FOX-7 molecule is introduced, the barrier height increases in 12 of the 18 cases investigated. Larger energy shifts are observed for dimers in which two α-FOX-7 molecules form intermolecular hydrogen bonds. Second, the size of the molecular cluster was systematically increased by introducing the neighboring α-FOX-7 molecules that had the largest impact on the barrier height. The largest cluster examined in this manuscript is the octamer. As shown in Figure 9, the shift of the energy barrier computed in the molecular cluster can be approximated as the summation of the energy barrier shifts computed with the corresponding dimers. Thus, the energy barrier demonstrates an additive relation between the molecular cluster and the dimers that construct it. Therefore, for the rest of the analysis, the shift of the potential energy introduced by the encapsulated environment is estimated to be the summation of the potential energy shifts calculated from all dimers in the first solvation shell.

Table 3. Potential Energy Shifts (kJ mol^{-1}) of Various Species as a Result of Introducing a Neighboring Molecule[a]

neighboring molecule	TS1	TS2	p3 + NH_2	i4 + NO_2	MSX-1	MSX-2	MSX-3
			Relative Energy in the Gas Phase with Respect to α-FOX-7				
	146.7[b]	76.5[b]	335.2[b]	174.2[b]	254.7[c]	211.2[c]	259.2[c]
			Energy Shift in the Dimer				
b1	0.4	−2.8	−3.3	2.4	1.0	−3.4	−0.2
b2	3.4	31.0	14.0	22.1	14.5	1.6	−2.6
b3	−2.0	3.7	8.1	1.5	1.5	1.8	−2.4
b4	−1.7	−1.5	−1.1	−3.6	−1.5	3.6	−7.3
b5	−1.8	−1.9	0.4	−2.1	−2.2	0.6	0.2
b6	3.0	10.4	7.9	0.4	−0.4	5.6	−0.7
m1	6.0	27.0	17.4	27.9	30.5	18.2	−10.0
m2	26.8	8.2	−3.4	27.0	−5.1	4.6	0.3
m3	−8.4	5.2	17.6	−8.3	3.1	2.6	−2.7
m4	3.0	13.5	21.4	7.9	11.8	−1.6	−5.0
m5	3.8	11.4	−7.1	5.6	5.1	−3.1	−2.1
m6	−0.7	5.0	1.3	−8.1	−4.2	1.4	2.1
t1	0.6	1.6	−2.6	4.2	−1.9	0.6	−2.7
t2	10.0	16.6	4.9	37.8	27.7	20.2	−10.6
t3	2.2	1.2	3.6	6.0	1.1	2.1	−2.4
t4	2.6	50.3	13.3	16.6	−4.7	−19.2	9.0
t5	−0.9	−5.4	1.5	−5.4	2.3	−1.3	0.7
t6	0.7	97.7	9.1	2.4	2.6	6.2	3.3
			Relative Energy in the Solid[d]				
	193	348	438	309	336	252	226

[a]**TS1** identifies the transition state between α-FOX-7 and **i1**, and **TS2** is the transition state between α-FOX-7 and **i3**. The neighboring molecule designations are displayed in Figure 8. The values for "total relative energy in solid" are utilized for Table 2 for the condensed phase columns of the computation prediction. [b]CCSD(T)-F12 with ZPE. [c]CASPT2 with ZPE. [d]±4.6 kJ mol^{-1}.

https://doi.org/10.1021/acs.jpca.2c02696
J. Phys. Chem. A XXXX, XXX, XXX−XXX

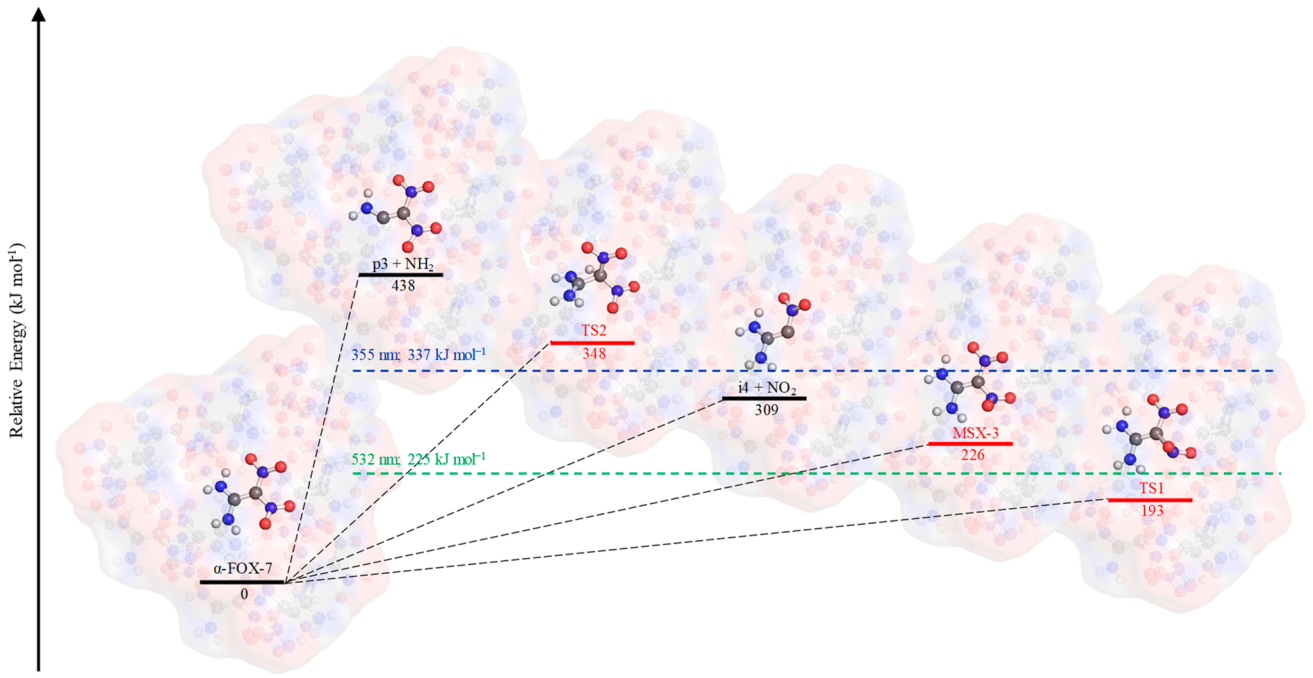

Figure 10. Extracted potential energy of key species following α-FOX-7 decomposition. **TS1** identifies the transition state between α-FOX-7 and **i1**, and **TS2** represents the transition state between α-FOX-7 and **i3**.

The potential energy shifts because of interactions with neighboring molecules immediately following α-FOX-7 on the potential energy surfaces are presented in the Table 3. The extracted potential energy profile of the decomposition of α-FOX-7 is shown in Figure 10. In the case that involves a gaseous product (e.g., NO, NO_2, or NH_2), the gaseous product was assumed to have left the cluster. As shown, the pathway of forming **p1** + NO involves overcoming **TS1**, a barrier of 193 kJ mol^{-1}. This barrier is accessible to both 355 nm (337 kJ mol^{-1}) and 532 nm (225 kJ mol^{-1}) photons. The endoergicity of forming **p3** + NH_2 is calculated to be 438 kJ mol^{-1}, which is inaccessible to 355 nm (337 kJ mol^{-1}) or 532 nm (225 kJ mol^{-1}) photons. The pathways involving the formation of nitrogen dioxide (NO_2) proceed through **i3**, eventually leading to **p2** + NO_2 or through **i4** + NO_2. The potential energy barrier of the step (**TS2**) to **i3** is 348 kJ mol^{-1}; therefore, it is blocked for the 355 nm (337 kJ mol^{-1}) and 532 nm (225 kJ mol^{-1}) photons. In regard to **i4** + NO_2 (309 kJ mol^{-1}), it is not accessible at 532 nm (225 kJ mol^{-1}) but is accessible, yet close in energy, to the 355 nm (337 kJ mol^{-1}) photons. The molecular oxygen formation pathway via **MSX-1** at 336 kJ mol^{-1} is only accessible to 355 nm (337 kJ mol^{-1}) photons. The molecular oxygen formation pathway via $O(^3P)$ recombination through **MSX-2** and **MSX-3** is found to be at 252 and 226 kJ mol^{-1}, respectively. Similar to **MSX-1**, **MSX-2** is still only accessible to 355 nm (337 kJ mol^{-1}) photons; however, the location of **MSX-3** (226 kJ mol^{-1}) is very close to the energy of the 532 nm (225 kJ mol^{-1}) photons and well below the energy of 355 nm (337 kJ mol^{-1}) photons. Given the error involved in the model mimicking the encapsulated environment, it is considered to be accessible at both 355 and 532 nm. The results of the gas phase and condensed phase predicted species compared with the experiments is summarized in Table 2.

As shown in the table, by simulating the encapsulated environment with a small cluster, the additive model greatly improves upon the gas phase calculation. This is especially true for the dissociation product of the 355 nm (337 kJ mol^{-1}) photolysis, in which all possible products are correctly predicted except for NO_2. In the actual solid phase environment, any newly generated nitrogen dioxide molecules would likely be trapped in the matrix, and the assumption involved in the molecular cluster calculation—that nitrogen dioxide has left the crystal once it is formed at 5 K—is only true for the surface layer of FOX-7. A trapped nitrogen dioxide molecule could recombine with **i4** and form **i1**, leading to the formation of **p1** + NO, which is detected by the experiment. Even in the cases where the prediction based on the condensed phase calculation does not agree with the experiment, the actual difference in energy is moderate. For example, the difference in energy to predict the formation of NO_2 is only 28 kJ mol^{-1}. This discrepancy could be the results of inherent errors involved in the calculations and the additive model of the molecular cluster and deserves attention in future research.

6. CONCLUSIONS

The UV photolysis of solid α-FOX-7 at 5 K with 355 and 532 nm photons was designed to unravel initial isomerization and decomposition pathways. Infrared spectroscopy revealed a nitro-to-nitrite isomerization of FOX-7 at 355 nm as evident from the observed −ONO moiety at 1610 cm^{-1}. Isomer-selective single photon ionization coupled with reflectron time-of-flight mass spectrometry (ReTOF-MS) documented the nitric oxide (NO) loss channel at 355 nm, whereas a residual gas analyzer detected molecular oxygen for the 355 and 532 nm photolysis at a ratio of 4.3 ± 0.3:1. Overall branching ratios for molecular oxygen versus nitric oxide were derived to be 700 ± 100:1 at 355 nm, suggesting that the photolysis of FOX-7 supplies its own oxidizer in the initial stage of decomposition. Merging the experimental observations with electronic structure calculations suggests that for 355 nm, the nitro-to-nitrite isomerization in FOX-7 represents the initial reaction

https://doi.org/10.1021/acs.jpca.2c02696
J. Phys. Chem. A XXXX, XXX, XXX−XXX

pathway followed by O—NO bond rupture of the nitrite moiety to nitric oxide (NO). In contrast to previous decomposition studies in our laboratory at 5 K involving nitromethane (CH_3NO_2)[76,78,79,81] and RDX,[34,35] no nitrogen dioxide (NO_2) was observed suggesting the absence of any C—NO_2 bond rupture process. The absence of the nitrogen dioxide channel is likely the result of the crystal structure of α-FOX-7 holding waved sheets of FOX-7 molecules linked by hydrogen bonding between oxygen atoms of the nitro group with hydrogen atoms of the amino group both inter- and intramolecularly. Even if a carbon−nitrogen bond rupture in the C—NO_2 moiety occurred at 355 nm, these hydrogen bonds may retain the nitrogen dioxide within the solid state in a geometrical orientation allowing a rapid radical−radical recombination at the carbon- and nitrogen-centered radicals. Further, although observed by Jiang et al.,[32] the nitrogen-containing decomposition products ammonia (NH_3), diazene (N_2H_2), and molecular nitrogen (N_2) were not observed in the present study. The formation of these molecules requires a carbon−nitrogen cleavage of the C—NH_2 moiety, which is not accessible energetically even at 355 nm through a single photon process. Finally, the computation confirms the detection of molecular oxygen at 355 and 532 nm and shows that atomic oxygen O(^{3}P) must be released by a nitro group that later combines to form molecular oxygen. For the first time, molecular oxygen (O_2) is detected as the decomposition product of α-FOX-7, making α-FOX-7 an energetic material that provides its own oxidant once the decomposition starts. Oxygen is expected to further react with FOX-7 and its decomposition products trapped in the matrix, which will lead to various reaction pathways. The condensed phase potential energy profile correlates well with the experiments, and by comparison with its gas phase counterpart, it highlights how the encapsulated environment dictates the mechanism of the reaction. Energetically favored pathways (e.g., FOX-7 → **i3** → **p2** + NO_2) found in the gas phase could be blocked because of the high energy required to break intermolecular hydrogen bonds present in the condensed phase, whereas other high-reaction-energy pathways in the gas phase could also be stabilized in the condensed phase and become energetically accessible (e.g., FOX-7 → O_2 + products).

■ ASSOCIATED CONTENT

Supporting Information

The Supporting Information is available free of charge at https://pubs.acs.org/doi/10.1021/acs.jpca.2c02696.

Potential energy surface of N_2H_2 isomers, geometric comparison between gas phase and crystalline FOX-7, infrared spectrum of FOX-7 at 300 K from 3500−6000 cm^{-1}, zwitterionic form of FOX-7, calculated adiabatic ionization energies, calculated fundamental infrared modes of intermediate i3, calculation of irradiation dose, synthesis and characterization data of FOX-7, and IR spectra and DTA measurement of FOX-7 (PDF)

■ AUTHOR INFORMATION

Corresponding Authors

Rui Sun − *Department of Chemistry, University of Hawaii, Honolulu, Hawaii 96822, United States;* orcid.org/0000-0003-0638-1353; Email: ruisun@hawaii.edu

Thomas M. Klapötke − *Department of Chemistry, Ludwig-Maximilian University of Munich, 81377 München, Germany*; Email: tmk@cup.uni-muenchen.de

Ralf I. Kaiser − *Department of Chemistry, University of Hawaii, Honolulu, Hawaii 96822, United States; W. M. Keck Research Laboratory in Astrochemistry, University of Hawaii, Honolulu, Hawaii 96822, United States;* orcid.org/0000-0002-7233-7206; Email: ralfk@hawaii.edu

Authors

Andrew M. Turner − *Department of Chemistry, University of Hawaii, Honolulu, Hawaii 96822, United States; W. M. Keck Research Laboratory in Astrochemistry, University of Hawaii, Honolulu, Hawaii 96822, United States*

Yuheng Luo − *Department of Chemistry, University of Hawaii, Honolulu, Hawaii 96822, United States;* orcid.org/0000-0002-3124-1179

Joshua H. Marks − *Department of Chemistry, University of Hawaii, Honolulu, Hawaii 96822, United States; W. M. Keck Research Laboratory in Astrochemistry, University of Hawaii, Honolulu, Hawaii 96822, United States*

Jasmin T. Lechner − *Department of Chemistry, Ludwig-Maximilian University of Munich, 81377 München, Germany*

Complete contact information is available at: https://pubs.acs.org/10.1021/acs.jpca.2c02696

Author Contributions

#A.M.T. and Y.L. contributed equally.

Notes

The authors declare no competing financial interest.

■ ACKNOWLEDGMENTS

The research reported in this manuscript is supported by the Office of Naval Research (grant number: A9550-21-1-0221). The authors appreciate the Information Technology Service (ITS) from the University of Hawaii at Manoa for the computational resources. We thank Zbigniew Dreger for advice about the solvation of FOX-7 in DMSO.

■ REFERENCES

(1) Fried, L. E.; Manaa, M. R.; Lewis, J. P. Modeling the Reactions of Energetic Materials in the Condensed Phase. *Overviews of Recent Research on Energetic Materials* **2005**, *16*, 275−301.

(2) Oxley, J. C. A Survey of the Thermal Stability of Energetic Materials. In *Theoretical and Computational Chemistry*; Politzer, P., Murray, J. S., Eds.; Elsevier, 2003; Vol. *12*, pp 5−48.

(3) Kozak, G. D. Factors Augmenting the Detonability of Energetic Materials. *Propellants, Explosives, Pyrotechnics* **2005**, *30*, 291−297.

(4) Singh, R. P.; Verma, R. D.; Meshri, D. T.; Shreeve, J. n. M. Energetic Nitrogen-Rich Salts and Ionic Liquids. *Angew. Chem., Int. Ed.* **2006**, *45*, 3584−3601.

(5) Sikder, A. K.; Sikder, N. A Review of Advanced High Performance, Insensitive and Thermally Stable Energetic Materials Emerging for Military and Space Applications. *Journal of Hazardous Materials* **2004**, *112*, 1−15.

(6) Badgujar, D. M.; Talawar, M. B.; Asthana, S. N.; Mahulikar, P. P. Advances in Science and Technology of Modern Energetic Materials: An Overview. *Journal of Hazardous Materials* **2008**, *151*, 289−305.

(7) Adams, G. F.; Shaw, R. W. Chemical Reactions in Energetic Materials. *Annu. Rev. Phys. Chem.* **1992**, *43*, 311−340.

(8) Brill, T. B.; James, K. J. Kinetics and Mechanisms of Thermal Decomposition of Nitroaromatic Explosives. *Chem. Rev.* **1993**, *93*, 2667−2692.
(9) Behrens, R. Thermal Decomposition Processes of Energetic Materials in the Condensed Phase at Low and Moderate Temperatures. *Overviews of Recent Research on Energetic Materials*; Advanced Series in Physical Chemistry; World Scientific, 2005; pp 29−73.
(10) Sorescu, D. C.; Boatz, J. A.; Thompson, D. L. Classical and Quantum-Mechanical Studies of Crystalline FOX-7 (1,1-Diamino-2,2-Dinitroethylene). *J. Phys. Chem. A* **2001**, *105*, 5010−5021.
(11) Majano, G.; Mintova, S.; Bein, T.; Klapötke, T. M. Confined Detection of High-Energy-Density Materials. *J. Phys. Chem. C* **2007**, *111*, 6694−6699.
(12) Klapötke, T. M. *Chemistry of High-Energy Materials*; de Gruyter, 2019.
(13) Mathieu, D. MATEO: A Software Package for the Molecular Design of Energetic Materials. *Journal of Hazardous Materials* **2010**, *176*, 313−322.
(14) Shteinberg, A. S.; Berlin, A. A.; Denisaev, A. A.; Mukasyan, A. S. Kinetics of Fast Reactions in Condensed Systems: Some Recent Results (an Autoreview). *International Journal of Self-Propagating High-Temperature Synthesis* **2011**, *20*, 259−265.
(15) Morton, R. J.; Kaiser, R. I. Kinetics of Suprathermal Hydrogen Atom Reactions with Saturated Hydrides in Planetary and Satellite Atmospheres. *Planetary and Space Science* **2003**, *51*, 365−373.
(16) Latypov, N. V.; Bergman, J.; Langlet, A.; Wellmar, U.; Bemm, U. Synthesis and Reactions of 1,1-Diamino-2,2-Dinitroethylene. *Tetrahedron* **1998**, *54*, 11525−11536.
(17) Yuan, B.; Yu, Z.; Bernstein, E. R. Initial Decomposition Mechanism for the Energy Release from Electronically Excited Energetic Materials: FOX-7 (1,1-Diamino-2,2-Dinitroethene). *J. Chem. Phys.* **2014**, *140*, 074708.
(18) Politzer, P.; Concha, M. C.; Grice, M. E.; Murray, J. S.; Lane, P. Computational Investigation of the Structures and Relative Stabilities of Amino/Nitro Derivatives of Ethylene. *Journal of Molecular Structure: THEOCHEM* **1998**, *452*, 75−83.
(19) Gindulyte, A.; Massa, L.; Huang, L.; Karle, J. Decomposition Mechanism of 1,1-Diamino Dinitroethylene (FOX-7): An Overview of the Quantum Chemical Calculation. In *Theoretical and Computational Chemistry*; Politzer, P., Murray, J. S., Eds.; Elsevier, 2003; Vol. *12*, pp 91−109.
(20) Zong, H.; Huang, Y.; Shu, Y.; Wang, X. Theoretical Study on the Initial Thermal Decomposition and Catalysis Effects of NO_2 on FOX-7. *Chin. J. Energet. Mater.* **2006**, *14*, 425−428.
(21) Kimmel, A. V.; Sushko, P. V.; Shluger, A. L.; Kuklja, M. M. Effect of Charged and Excited States on the Decomposition of 1,1-Diamino-2,2-Dinitroethylene Molecules. *J. Chem. Phys.* **2007**, *126*, 234711.
(22) Booth, R. S.; Butler, L. J. Thermal Decomposition Pathways for 1,1-Diamino-2,2-Dinitroethene (FOX-7). *J. Chem. Phys.* **2014**, *141*, 134315.
(23) Türker, L.; Varış, S. Effects of Epoxidation and Nitration on Ballistic Properties of FOX-7 - a DFT Study. *Zeitschrift für anorganische und allgemeine Chemie* **2013**, *639*, 982−987.
(24) Ma, Y.; Lv, M.; Shang, F.; Zhang, C.; Liu, J.; Zhou, P. Mechanistic Investigation on the Initial Thermal Decomposition of Energetic Materials FOX-7 and RDX in the Crystal and Gas Phase: An MM/DFT-Based ONIOM Calculation. *J. Phys. Chem. A* **2022**, *126*, 1666.
(25) Jones, D.; Vachon, M.; Wang, R.; Kwok, Q. Preliminary Studies on the Thermal Properties of FOX-7; *Proc. NATAS Annu. Conf. Therm. Anal. Appl. 32nd*; NATAS, 2004; pp 1−105.17.
(26) Jin, P.-G.; Chang, H.; Chen, Z.-Q. Studies on Kinetics and Mechanisms of Thermal Decomposition of 1,1-Diamino-2,2-Dinitroethylene (FOX-7). *Explosion Shock Waves* **2006**, *26*, 528.
(27) Civiš, M.; Civiš, S.; Sovová, K.; Dryahina, K.; Španěl, P.; Kyncl, M. Laser Ablation of FOX-7: Proposed Mechanism of Decomposition. *Anal. Chem.* **2011**, *83*, 1069−1077.
(28) Zhang, J.-D.; Zhang, L.-L. Theoretical Study on the Mechanism of the Reaction of FOX-7 with OH and NO_2 Radicals: Bimolecular Reactions with Low Barrier During the Decomposition of FOX-7. *Mol. Phys.* **2017**, *115*, 2951−2960.
(29) Winey, J. M.; Zimmerman, K.; Dreger, Z. A.; Gupta, Y. M. Structural Transformation and Chemical Stability of a Shock-Compressed Insensitive High Explosive Single Crystal: Time-Resolved Raman Spectroscopy. *J. Phys. Chem. A* **2020**, *124*, 6521−6527.
(30) Zheng, Z.; Xu, J.; Zhao, J. First-Principles Studies on the Thermal Decomposition Behavior of FOX-7. *High Pressure Research* **2010**, *30*, 301−309.
(31) Liu, Y.; Li, F.; Sun, H. Thermal Decomposition of FOX-7 Studied by Ab Initio Molecular Dynamics Simulations. *Theor. Chem. Acc.* **2014**, *133*, 1567.
(32) Jiang, L.; Fu, X.; Zhou, Z.; Zhang, C.; Li, J.; Qi, F.; Fan, X.; Zhang, G. Study of the Thermal Decomposition Mechanism of FOX-7 by Molecular Dynamics Simulation and Online Photoionization Mass Spectrometry. *RSC Adv.* **2020**, *10*, 21147−21157.
(33) Rashkeev, S. N.; Kuklja, M. M.; Zerilli, F. J. Electronic Excitations and Decomposition of 1,1-Diamino-2,2-Dinitroethylene. *Appl. Phys. Lett.* **2003**, *82*, 1371−1373.
(34) Singh, S. K.; La Jeunesse, J.; Vuppuluri, V.; Son, S. F.; Sun, B.-J.; Chen, Y.-L.; Chang, A. H. H.; Mebel, A. M.; Kaiser, R. I. The Elusive Ketene (H_2CCO) Channel in the Infrared Multiphoton Dissociation of Solid 1,3,5-Trinitro-1,3,5-Triazinane (RDX). *ChemPhysChem* **2020**, *21*, 837−842.
(35) Singh, S. K.; Vuppuluri, V.; Son, S. F.; Kaiser, R. I. Investigating the Photochemical Decomposition of Solid 1,3,5-Trinitro-1,3,5-Triazinane (RDX). *J. Phys. Chem. A* **2020**, *124*, 6801−6823.
(36) Manaa, M. R. Determination of Adiabatic Ionization Potentials and Electron Affinities of Energetic Molecules with the Gaussian-4 Method. *Chem. Phys. Lett.* **2017**, *678*, 102−106.
(37) Latypov, N. V.; Johansson, M.; Holmgren, E.; Sizova, E. V.; Sizov, V. V.; Bellamy, A. J. On the Synthesis of 1,1-Diamino-2,2-Dinitroethene (FOX-7) by Nitration of 4,6-Dihydroxy-2-Methylpyrimidine. *Org. Process Res. Dev.* **2007**, *11*, 56−59.
(38) Astrat'ev, A. A.; Dashko, D. V.; Mershin, A. Y.; Stepanov, A. I.; Urazgil'deev, N. A. Some Specific Features of Acid Nitration of 2-Substituted 4,6-Dihydroxypyrimidines. Nucleophilic Cleavage of the Nitration Products. *Russ. J. Org. Chem.* **2001**, *37*, 729−733.
(39) Jones, B. M.; Kaiser, R. I. Application of Reflectron Time-of-Flight Mass Spectroscopy in the Analysis of Astrophysically Relevant Ices Exposed to Ionization Radiation: Methane (CH_4) and D_4-Methane (CD_4) as a Case Study. *J. Phys. Chem. Lett.* **2013**, *4*, 1965−1971.
(40) Turner, A. M.; Kaiser, R. I. Exploiting Photoionization Reflectron Time-of-Flight Mass Spectrometry to Explore Molecular Mass Growth Processes to Complex Organic Molecules in Interstellar and Solar System Ice Analogs. *Acc. Chem. Res.* **2020**, *53*, 2791−2805.
(41) Hilbig, R.; Wallenstein, R. Narrowband Tunable VUV Radiation Generated by Nonresonant Sum-and Difference-Frequency Mixing in Xenon and Krypton. *Applied optics* **1982**, *21*, 913−917.
(42) Hilbig, R.; Hilber, G.; Lago, A.; Wolff, B.; Wallenstein, R. Tunable Coherent VUV Radiation Generated by Nonlinear Optical Frequency Conversion in Gases. *Nonlinear Optics and Applications*; International Society for Optics and Photonics, 1986; pp 48−57.
(43) Zhao, Y.; Truhlar, D. G. The M06 Suite of Density Functionals for Main Group Thermochemistry, Thermochemical Kinetics, Noncovalent Interactions, Excited States, and Transition Elements: Two New Functionals and Systematic Testing of Four M06-Class Functionals and 12 Other Functionals. *Theor. Chem. Acc.* **2008**, *120*, 215−241.
(44) Grimme, S.; Antony, J.; Ehrlich, S.; Krieg, H. A Consistent and Accurate Ab Initio Parametrization of Density Functional Dispersion Correction (DFT-D) for the 94 Elements H-Pu. *J. Chem. Phys.* **2010**, *132*, 154104.
(45) Weigend, F.; Ahlrichs, R. Balanced Basis Sets of Split Valence, Triple Zeta Valence and Quadruple Zeta Valence Quality for H to Rn:

https://doi.org/10.1021/acs.jpca.2c02696
J. Phys. Chem. A XXXX, XXX, XXX−XXX

Design and Assessment of Accuracy. *Phys. Chem. Chem. Phys.* **2005**, *7*, 3297−3305.
(46) Valiev, M.; Bylaska, E. J.; Govind, N.; Kowalski, K.; Straatsma, T. P.; Van Dam, H. J. J.; Wang, D.; Nieplocha, J.; Apra, E.; Windus, T. L.; de Jong, W. A. NWChem: A Comprehensive and Scalable Open-Source Solution for Large Scale Molecular Simulations. *Comput. Phys. Commun.* **2010**, *181*, 1477−1489.
(47) Fukui, K. Formulation of the Reaction Coordinate. *J. Phys. Chem.* **1970**, *74*, 4161−4163.
(48) Maeda, S.; Harabuchi, Y.; Ono, Y.; Taketsugu, T.; Morokuma, K. Intrinsic Reaction Coordinate: Calculation, Bifurcation, and Automated Search. *Int. J. Quantum Chem.* **2015**, *115*, 258−269.
(49) Ischtwan, J.; Collins, M. A. Determination of the Intrinsic Reaction Coordinate: Comparison of Gradient and Local Quadratic Approximation Methods. *J. Chem. Phys.* **1988**, *89*, 2881−2885.
(50) Raghavachari, K.; Trucks, G. W.; Pople, J. A.; Head-Gordon, M. A Fifth-Order Perturbation Comparison of Electron Correlation Theories. *Chem. Phys. Lett.* **1989**, *157*, 479−483.
(51) Adler, T. B.; Knizia, G.; Werner, H.-J. A Simple and Efficient CCSD(T)-F12 Approximation. *J. Chem. Phys.* **2007**, *127*, 221106.
(52) Peterson, K. A.; Adler, T. B.; Werner, H.-J. Systematically Convergent Basis Sets for Explicitly Correlated Wavefunctions: The Atoms H, He, B-Ne, and Al-Ar. *J. Chem. Phys.* **2008**, *128*, 084102.
(53) Knizia, G.; Adler, T. B.; Werner, H.-J. Simplified CCSD(T)-F12 Methods: Theory and Benchmarks. *J. Chem. Phys.* **2009**, *130*, 054104.
(54) Adler, T. B.; Werner, H.-J. An Explicitly Correlated Local Coupled Cluster Method for Calculations of Large Molecules Close to the Basis Set Limit. *J. Chem. Phys.* **2011**, *135*, 144117.
(55) Werner, H. J.; Knowles, P. J.; Knizia, G.; Manby, F. R.; Schütz, M. Molpro: A General-Purpose Quantum Chemistry Program Package. *Wiley Interdisciplinary Rev.: Comput. Mol. Sci.* **2012**, *2* (2), 242−253.
(56) Werner, H.-J.; Knowles, P. J.; Manby, F. R.; Black, J. A.; Doll, K.; Heßelmann, A.; Kats, D.; Köhn, A.; Korona, T.; Kreplin, D. A.; et al. The Molpro Quantum Chemistry Package. *J. Chem. Phys.* **2020**, *152*, 144107.
(57) Dunning, T. H., Jr. Gaussian Basis Sets for Use in Correlated Molecular Calculations. I. The Atoms Boron through Neon and Hydrogen. *J. Chem. Phys.* **1989**, *90*, 1007−1023.
(58) Varandas, A. J. C. Basis-Set Extrapolation of the Correlation Energy. *J. Chem. Phys.* **2000**, *113*, 8880−8887.
(59) Evers, J.; Klapötke, T. M.; Mayer, P.; Oehlinger, G.; Welch, J. A- and B-FOX-7, Polymorphs of a High Energy Density Material, Studied by X-Ray Single Crystal and Powder Investigations in the Temperature Range from 200 to 423 K. *Inorg. Chem.* **2006**, *45*, 4996−5007.
(60) Celani, P.; Werner, H.-J. Multireference Perturbation Theory for Large Restricted and Selected Active Space Reference Wave Functions. *J. Chem. Phys.* **2000**, *112*, 5546−5557.
(61) Győrffy, W.; Shiozaki, T.; Knizia, G.; Werner, H.-J. Analytical Energy Gradients for Second-Order Multireference Perturbation Theory Using Density Fitting. *J. Chem. Phys.* **2013**, *138*, 104104.
(62) Roos, B. O.; Taylor, P. R.; Sigbahn, P. E. M. A Complete Active Space SCF Method (CASSCF) Using a Density Matrix Formulated Super-CI Approach. *Chem. Phys.* **1980**, *48*, 157−173.
(63) Farazdel, A.; Dupuis, M. On the Determination of the Minimum on the Crossing Seam of Two Potential Energy Surfaces. *J. Comput. Chem.* **1991**, *12*, 276−282.
(64) Kushtaev, A. A.; Yudin, N. V.; Kondakova, N. N.; Ilicheva, N. N.; Vu, T. Q.; Zbarskiy, V. L. Investigation of FOX-7 Polymorphs: New Polymorphs - ϵ and Z. *ChemistrySelect* **2021**, *6*, 12562−12570.
(65) Zhang, H.-L.; Yu, L.; Zhang, H.-B.; Li, S.-C.; Zhu, C.-H.; Xu, J.-J.; Yang, S.-Y.; Li, J.-S. Investigation of the Phase Transitions of FOX-7 by Temperature-Dependent FTIR Spectroscopy. *Chin. J. Energet. Mater.* **2016**, *24* (9), 880−885.
(66) Fan, X.-Z.; Li, J.-Z.; Liu, Z.-R. Thermal Behavior of 1,1-Diamino-2,2-Dinitroethylene. *J. Phys. Chem. A* **2007**, *111*, 13291−13295.
(67) Trzciński, W.; Belaada, A. 1, 1-Diamino-2, 2-Dinitroethene (DADNE, FOX-7)-Properties and Formulations (a Review). *Central European Journal of Energetic Materials* **2016**, *13*, 527−544.
(68) Bemm, U.; Östmark, H. 1, 1-Diamino-2, 2-Dinitroethylene: A Novel Energetic Material with Infinite Layers in Two Dimensions. *Acta Crystallogr. Sect. C: Cryst. Struct. Commun.* **1998**, *54*, 1997−1999.
(69) Su, Y.; Fan, J.; Zheng, Z.; Zhao, J. Uniaxial Compression Behavior and Spectroscopic Properties of Energetic 1,1-Diamino-2,2-Dinitroethylene (FOX-7) Crystals from Density Functional Theory Calculations. *Progress in Natural Science: Materials International* **2019**, *29*, 329−334.
(70) Averkiev, B. B.; Dreger, Z. A.; Chaudhuri, S. Density Functional Theory Calculations of Pressure Effects on the Structure and Vibrations of 1,1-Diamino-2,2-Dinitroethene (FOX-7). *J. Phys. Chem. A* **2014**, *118*, 10002−10010.
(71) Dreger, Z. A.; Tao, Y.; Gupta, Y. M. High-Pressure Vibrational and Polymorphic Response of 1,1-Diamino-2,2-Dinitroethene Single Crystals: Raman Spectroscopy. *J. Phys. Chem. A* **2014**, *118*, 5002−5012.
(72) Huang, J.; Zhou, C.; Zhang, L.; Wang, B.; Ma, Q.; Li, X. Effects of Five Kinds of Commonly Used Single-Compound Explosives on Crystal Phase Transformation of FOX-7. *Chin. J. Energet. Mater.* **2016**, *24* (10), 960−964.
(73) Šimková, L.; Šoral, M.; Lušpai, K.; Ludvík, J. Spectroscopic Characterization of Different Structural Forms of the New Promising Energetic Material FOX-7 in Different Solvents. *J. Mol. Struct.* **2015**, *1083*, 10−16.
(74) *Electron-Impact Ionization Cross Sections*; Physical Measurement Laboratory, NIST; https://www.nist.gov/pml (accessed 2022).
(75) Muya, J. T.; Chung, H.; Lee, S. U. Theoretical Investigation on the Ground State Properties of the Hexaamminecobalt (III) and Nitro-Nitrito Linkage Isomerism in Pentaamminecobalt (III) in Vacuo. *RSC Adv.* **2018**, *8*, 3328−3342.
(76) Góbi, S.; Crandall, P. B.; Maksyutenko, P.; Förstel, M.; Kaiser, R. I. Accessing the Nitromethane (CH_3NO_2) Potential Energy Surface in Methanol (CH_3OH)-Nitrogen Monoxide (NO) Ices Exposed to Ionizing Radiation: An FTIR and Pi-Retof-Ms Investigation. *J. Phys. Chem. A* **2018**, *122*, 2329−2343.
(77) Ciofini, I.; Adamo, C. Intrinsic and Environmental Effects on the Kinetic and Thermodynamics of Linkage Isomerization in Nitritopentaamminecobalt(III) Complex. *J. Phys. Chem. A* **2001**, *105*, 1086−1092.
(78) Maksyutenko, P.; Muzangwa, L. G.; Jones, B. M.; Kaiser, R. I. Lyman Alpha Photolysis of Solid Nitromethane (CH_3NO_2) and D_3-Nitromethane (CD_3NO_2) - Untangling the Reaction Mechanisms Involved in the Decomposition of Model Energetic Materials. *Phys. Chem. Chem. Phys.* **2015**, *17*, 7514−7527.
(79) Kaiser, R. I.; Maksyutenko, P. Novel Reaction Mechanisms Pathways in the Electron Induced Decomposition of Solid Nitromethane (CH_3NO_2) and D3-Nitromethane (CD_3NO_2). *J. Phys. Chem. C* **2015**, *119*, 14653−14668.
(80) Bodenbinder, M.; Ulic, S. E.; Willner, H. A Gas phase and Matrix Isolation Study of the Equilibrium CH_3ONO (Cis) - CH_3ONO (Trans) by FTIR Spectroscopy. *J. Phys. Chem.* **1994**, *98*, 6441−6444.
(81) Singh, S. K.; Kaiser, R. I. A Vacuum Ultraviolet Photoionization Study on the Isomerization, Decomposition, and Molecular Mass Growth Processes in Solid Nitromethane (CH_3NO_2). *Chem. Phys. Lett.* **2021**, *766*, 138343.

https://doi.org/10.1021/acs.jpca.2c02696
J. Phys. Chem. A XXXX, XXX, XXX−XXX